clean technologies

MDPI

Article

A Numerical Analysis of the Effects of Supercritical CO_2 Injection on CO_2 Storage Capacities of Geological Formations

Kamal Jawher Khudaida * and Diganta Bhusan Das *

Department of Chemical Engineering, Loughborough University, Loughborough LE11 3TU, UK
* Correspondence: kjkamal2014@gmail.com (K.J.K.); D.B.Das@lboro.ac.uk (D.B.D.)

Received: 31 May 2020; Accepted: 20 August 2020; Published: 1 September 2020

Abstract: One of the most promising means of reducing carbon content in the atmosphere, which is aimed at tackling the threats of global warming, is injecting carbon dioxide (CO_2) into deep saline aquifers (DSAs). Keeping this in mind, this research aims to investigate the effects of various injection schemes/scenarios and aquifer characteristics with a particular view to enhance the current understanding of the key permanent sequestration mechanisms, namely, residual and solubility trapping of CO_2. The paper also aims to study the influence of different injection scenarios and flow conditions on the CO_2 storage capacity and efficiency of DSAs. Furthermore, a specific term of the permanent capacity and efficiency factor of CO_2 immobilization in sedimentary formations is introduced to help facilitate the above analysis. Analyses for the effects of various injection schemes/scenarios and aquifer characteristics on enhancing the key permanent sequestration mechanisms is examined through a series of numerical simulations employed on 3D homogeneous and heterogeneous aquifers based on the geological settings for Sleipner Vest Field, which is located in the Norwegian part of the North Sea. The simulation results highlight the effects of heterogeneity, permeability isotropy, injection orientation and methodology, and domain-grid refinement on the capillary pressure–saturation relationships and the amounts of integrated CO_2 throughout the timeline of the simulation via different trapping mechanisms (solubility, residual and structural) and accordingly affect the efficiency of CO_2 sequestration. The results have shown that heterogeneity increases the residual trapping of CO_2, while homogeneous formations promote more CO_2 dissolution because fluid flows faster in homogeneous porous media, inducing more contact with fresh brine, leading to higher dissolution rates of CO_2 compared to those in heterogeneous porous medium, which limits fluid seepage. Cyclic injection has been shown to have more influence on heterogenous domains as it increases the capillary pressure, which forces more CO_2 into smaller-sized pores to be trapped and exposed to dissolution in the brine at later stages of storage. Storage efficiency increases proportionally with the vertical-to-horizontal permeability ratio of geological formations because higher ratios facilitate the further extent of the gas plume and increases the solubility trapping of the integrated gas. The developed methodology and the presented results are expected to play key roles in providing further insights for assessing the feasibility of various geological formations for CO_2 storage.

Keywords: geological sequestration; CO_2 storage capacity; CO_2 storage efficiency; CO_2 sequestration; deep saline aquifers

1. Introduction

Injecting CO_2 into deep saline aquifers (DSAs) has been proposed as one of the most viable means of tackling global warming [1]. This is because the technology has developed sufficiently due to the

experience gained from oil and gas exploration and waste disposal methodologies. Moreover, the DSAs offer more extensive storage potential than other geological formations, such as oil and gas fields or coal seams [1]. Consequently, many studies have been conducted to assess their storage capacity and efficiency to safely sequester the injected gas [2–8].

As discussed earlier in our previous works [9,10], CO_2 storage methodology in saline aquifers can be categorised into hydrodynamic and chemical mechanisms. The first one includes the structural and residual trapping of CO_2 within the aquifer pore space, while the second one comprises of the solubility and mineral trapping of CO_2.

Two important factors that should be considered while assessing the suitability of an aquifer for sequestering CO_2 are its capacity and injectivity. They should allow for the safer and cost-effective storage of large amounts of the disposed gas [11]. Additionally, hydrostatic conditions play a crucial role in increasing the storage of saline aquifers because the higher pressure in deeper formations induces gas compression, resulting in more storage of CO_2 in a specific volume of the aquifer [12–14]. In this regard, the integrity of the caprock with low permeability is an essential consideration because any existing faults or cracks in the aquifer rock will result in the injected gas escaping to the surface. Porosity and permeability of the formation have significant influence on the selection of the appropriate site for carbon storage because the higher permeability of a medium allows fluids to migrate easily through the better-connected pores away from the injection well, which subsequently magnifies the capacity and efficiency of the aquifer to store CO_2 [15–18].

Theoretically, the storage capacity of an aquifer is the substantial limit of CO_2 that can be admitted into it [19,20]. However, this limit is not practically achievable due to various geological factors and engineering barriers (e.g., pore connectivity, lack of geological data, economic feasibility, legal regulations and infrastructure benchmarks). Therefore, a term called effective storage capacity has been coined [21,22], which has been a subject of a number of studies using different calculation methods. These methods involve the use of volumetric and compressibility methods [23–25], mathematical models [26], dimensional analyses [27], analytical investigations [28] and numerical modelling [29,30] to assess the efficiency of geological formations to sequester CO_2. Most of these studies are theoretical or analytical in nature based on 2D models that seem to lack sufficient interests for practical employment. Detailed comparison studies have been conducted to evaluate the impact of a variety of approaches and methodologies on estimating CO_2 sequestration in geological formations [20,31,32].

One basic estimation method, which is widely adopted, is the U.S. Department of Energy (US-DOE) method. As explained in detail by Goodman et al. [33], the method assumes an infinitive boundary and defines the efficiency of an aquifer to store CO_2 by the pore volume that is available to be occupied by the injected gas. It determines the CO_2 mass storage capacity and efficiency for an aquifer as:

$$G_{CO_2} = A_t h_g \varnothing_t \rho_{CO_2} E_{aq} \quad (1)$$

where A_t is the total cross-sectional area of the domain, h_g defines the gross thickness of the formation, $\varnothing_t$ is the total porosity of the rock, ρ_{CO_2} and E_{aq} represent the density of the injected CO_2 and the storage efficiency of the aquifer, respectively.

An earlier approach, proposed by Zhou et al. [23] predicts the pressure build-up history and the impact on the actual storage efficiency in response to the CO_2 injection process. The authors define the storage efficiency factor as the volumetric fraction of the sequestered CO_2 per unit volume of pores in the potential domain. In spite of achieving good agreement between the analytical results and the numerically predicted values, the authors state that this method is not suitable for geological formations of low permeability that lead to lower injectivity, and creates more non-uniformity in the pressure build-up within the simulated domain. This is due to many simplifications and assumptions in the analytical solutions in their research work.

Another method, developed by Szulczewski [34], considers both the residual and solubility trapping mechanisms in addition to the CO_2 migration capacity. The method is applicable to both open-boundary and pressure-limited systems. Additionally, this method counts the net thickness of the

aquifer to calculate the pore volume instead of the gross thickness in heterogeneous domains. This is because most of the injected CO_2 targets the high-porosity layers, such as sandstone or carbonate rocks, rather than any intermingled layers of shale or clay that store negligible amounts of the injected gas.

For open-boundary systems, the total mass of CO_2 (C_t) stored in an aquifer can be determined by [34]:

$$C_t = \rho_g L_t W H \varnothing (1 - S_{wc}) \frac{2}{\varepsilon_T} \tag{2}$$

where ρ_g is the density of CO_2 at prevailing temperature and pressure, L_t is the total length of the aquifer, W is the width of the well, H is the net thickness of the aquifer $\varnothing$ is the porosity of the rock, S_{wc} is the connate water saturation and $\frac{2}{\varepsilon_T}$ is the storage efficiency factor.

If the aquifer is classified as a pressure-limited system, the CO_2 mass is calculated as follows [34]:

$$C_p = \rho_g H W \sqrt{\frac{k_{aq} c T}{\mu_w}} \frac{P_{fraq} - (p_o + \overline{\rho_w} g D)}{4 \widetilde{p}_{max}} \tag{3}$$

where k_{aq} is the permeability of the aquifer, c is the compressibility, T is the temperature, μ_w is the brine viscosity, P_{fraq} is the fracture pressure of the rock, p_o is the hydrostatic pressure, $\overline{\rho_w}$ is the average density of brine, g is the gravitational acceleration, D is the depth to the top of the aquifer and $\widetilde{p}_{max}$ represents the maximum dimensionless pressure in the system which needs to be determined numerically, solving a different set of partial differential equations (PDEs) for the pressure-limited flow system [34].

Several techniques can be used to increase the capacity and efficiency of CO_2 sequestration in saline aquifers that will consequently support the efforts by the Intergovernmental Panel on Climate Change (IPCC) to incite policy makers with the importance of deploying carbon capture and sequestration (CCS) as one of the cost effective technologies for confronting climate change and global warming concerns.

Geological formation capacity can be increased by improving the injectivity through increasing the injection mass flow rate or pressure to compensate the loss of permeability due to salt precipitation in the well vicinity. Furthermore, injecting into adjacent layers with high permeability helps with attenuating pressure build-up and, consequently, higher injection rates can be employed [35,36].

Using horizontal injection wells instead of vertical ones is one of the methods implemented to increase the injectivity and capacity of aquifers because it helps to diminish the pressure-build-up peaks around the injection well and spread pressure uniformly within the domain. Deploying this technique requires the determination of the minimum length of the horizontal well that is dependent on the effective radius of pressure disturbance around the vertical injection well [37–40].

It has been evidenced that the solubility of CO_2 into brine can be accelerated by injecting slugs of fresh brine on top of the storage formation during and after CO_2 injection. This can increase CO_2 dissolution by more than 40% within a period of 200 years, which reduces the risk of CO_2 leakage in long-term sequestration, according to the study by Hassanzadeh et al. [41]. The study also investigated further factors that have significant impact on increasing the storage efficiency in saline aquifers, including optimizing the rate of the injected brine and transporting the injected and existing fluids within the reservoir in addition to the effect of aquifer properties, such as thickness, vertical anisotropy and layers of heterogeneity included within the media.

In their work, De Silva and Ranjith [39] concluded that, while using horizontal injection wells in the absence of chase brine injection improves the storage of aquifers, vertical injection wells with chase brine injection performs better storage efficiency. However, the authors suggest that the injection process should be carried out over the whole thickness of the aquifer to maximize the storage capacity. In contrast, Khudaida and Das [9] observed that injecting CO_2 into the lower section of a reservoir enhances the solubility trapping mechanism and subsequently increases the storage efficiency.

Introducing hydraulic fractures in formation rock can improve the injectivity by increasing the effective permeability of the aquifer, which facilitates migration and, consequently, preserves more

contact between the injected CO_2 and the existing brine, in addition to preventing any pressure build-up within the aquifer. However, this technique needs a detailed characterization of the formation and has to be implemented with extra care to avoid causing any gas leakage [38].

Keeping the above discussions in mind, this work aims to provide further understanding on how to assess the feasibility of a potential storage site by investigating the behaviour and migration of CO_2-brine as a two-phase flow system in porous geological formations under various injection conditions and scenarios. It also demonstrates the effects of various site characteristics, such as heterogeneity and anisotropy, on the injectivity and safe storage of the injected CO_2. To aid the above, the capillary pressure relationships for CO_2-brine as a two-phase flow is also studied. It is envisaged that the results will address the applicability of different injection techniques in terms of orientation and continuity to enhance the capacity and efficiency of sequestering CO_2 in geological formations.

2. Modelling Setup

To assess the storage capacity and efficiency of an unconfined aquifer (i.e., migration-limited domain), a hypothetical cylindrical computational domain, extending from 0.3 m (the radius of the injection-well case) to 6000 m laterally and 96 m vertically, was simulated with two types of numerical grid resolutions, namely, coarse and fine grids. For the coarse-grid, the domain was horizontally discretized into 88 grid-blocks with a finer mesh in the vicinity of the injection well, which became gradually coarser further away. Vertically, the domain was discretized into 24 blocks of 4 m high. This mesh refinement has made 2112 elements as shown in Figure 1. For the fine resolution, the grid spacing was increased by 100% in both directions, producing 8448 cells. Supercritical CO_2 ($scrCO_2$) was injected into the centre of the domain at a constant rate of 32.0 kg/s (about 1 MMT/year), which represents a typical benchmark value [38], via a number of cells either at the bottom section or through the whole thickness of the reservoir.

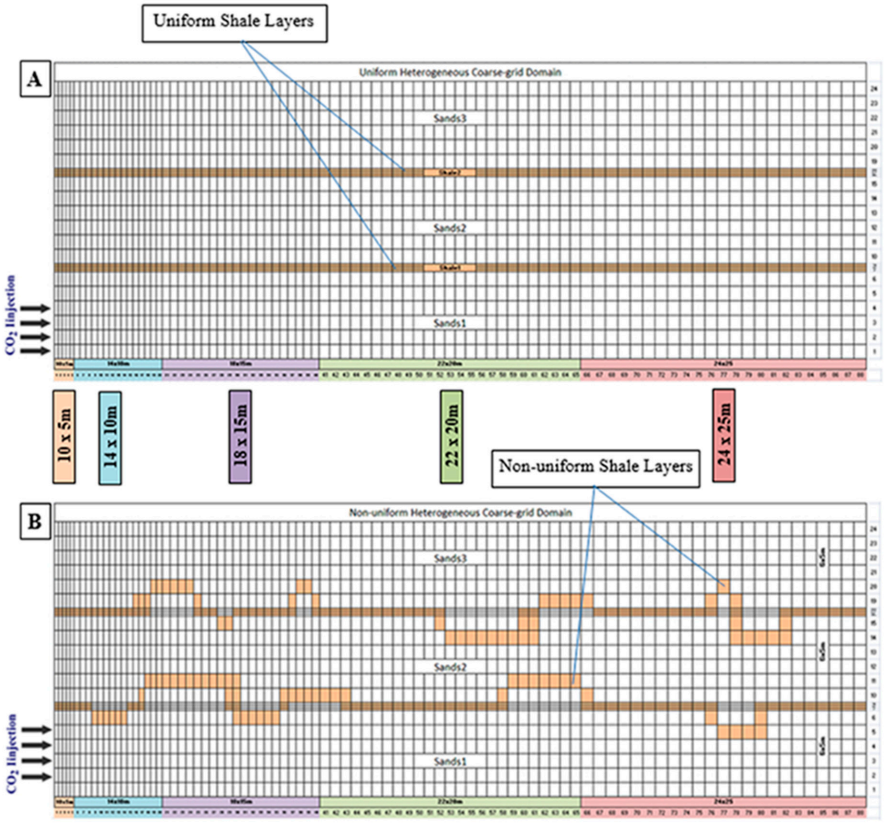

Figure 1. A schematic 2D diagram of the modelled heterogeneous domains: (**A**) uniform heterogeneity; (**B**) non-uniform heterogeneity.

Heterogeneity is defined as the variability of porosity/permeability within the simulated domain and is usually quantified using various geostatistical techniques, including the Lorenz coefficient (*Lc*) and the coefficient of variation (*Cv*) methods that are commonly used in establishing porosity and permeability models in exploration. For this study, this variability was not calculated because the simulation parameters were taken from geological settings for Sleipner Vest Field (Tables 1 and 2).

Table 1. Lithostratigraphic division and petrophysical parameters from Sleipner Vest Field, after [42]. These are model parameters used in this study; however, the developed methodology is generic and may be applied in other geological formations.

Layer	Units	Sand 1	Sand 2	Sand 3	Shale 1	Shale 2
Thickness	(m)	30	30	30	3	3
Porosity	-	0.35			0.1025	
Horizontal permeability	(md) (m^2)	304 3.0×10^{-13}			10.13 0.1×10^{-13}	
Vertical permeability	(md) (m^2)	304 3.0×10^{-13}			10.13 0.1×10^{-13}	
Density	(kg/m^3)	2650				
Pore Compressibility	(Pa^{-1})	4.5×10^{-10}				
Aquifer pressure	(MPa)	11.2				
Pressure gradient	(KPa/m)	10.012				
Aquifer temperature	(°C)	37				
Salinity (mass fraction)	-	0.032				
Aquifer depth	(m)	800–1100				
Water depth	(m)	110				

Table 2. Capillary pressure–saturation; permeability functions parameters of the simulated aquifer, after [42,43].

Description	Symbol	Value	Units
Irreducible aqueous saturation [42]	S_{lr}	0.2	-
Irreducible gas saturation [42]	S_{gr}	0.05	-
Saturation function parameters for (Sand) [42]	α	2.735	M^{-1}
Saturation function parameters for (Shale) [42]	α	0.158	M^{-1}
Saturation function parameters [43]	m	0.4	-
	n	1.667	-
Pore index parameter $\lambda = \frac{m}{1-m}\left(1-0.5^{\frac{1}{m}}\right) = n-1$	λ	0.667	-
Maximum residual gas saturation for aquifer [43]	S_{grm}	0.208	-
Maximum residual gas saturation for aquitard [43]	S_{grm}	0.448	-

2.1. Parameters and Calculations

STOMP-CO_2 simulation code [42] was used to carry out the simulation runs in this research work and conduct the P_c-S_w calculations. This has been discussed earlier [9,42] and therefore it is not discussed in detail in this paper and, additionally, the simulation code results were validated through a reasonable mapping with a lab-scale setup which was described in detail in a dedicated section of previous research by the authors [44]. The simulation parameters used in this work are based on the geological settings for the Sleipner Vest Field, which is located in the Norwegian part of the North Sea at an approximate depth of 1100 m. It is identified to be one of the typical CO_2 disposal sites offering anticipated hydrostatic conditions to keep the injected CO_2 in supercritical conditions. Moreover, this depth is far enough away from the fresh water sources, which are usually located at around a 500 m depth. All petrophysical parameters and formulations factors are listed in Tables 1 and 2. CO_2 properties adopted in the simulation were arranged in a data table developed from the equation of state (EOS) by Span and Wagner [45], which is widely considered to be an accurate reference EOS for

CO_2 for its ability to provide accurate results in the most technically relevant pressures up to 30 MPa and temperatures up to 523 K, the conditions that are common in the geological sequestration of CO_2.

The Span and Wagner equation is based on an extensive range of fitted experimental thermal properties in the single-phase region, the liquid–vapour saturation curve, the speed of sound, the specific heat capacities, the specific internal energy and the Joule–Thomson coefficient [46]. This equation is expressed in the form of the Helmholtz energy (ϕ) as follows:

$$\phi(\delta, \mathcal{T}) = \phi(\delta, \mathcal{T}) + \phi^r(\delta, \mathcal{T}) \tag{4}$$

where $\phi = \rho/\rho_c$, $\mathcal{T} = T_c/T$, ρ_c and T_c are the critical density and critical temperature of CO_2, respectively. ϕ is the ideal gas part of the Helmholtz energy and ϕ^r is the residual part of the Helmholtz energy. The two parts of the Helmholtz energy (the basic and phase diagram elements) of this equation of state are explained in detail in the literature published by Span and Wagner [45] and are not repeated in this study. The Span and Wagner EOS has been employed in this research to calculate the density of CO_2 at different simulation conditions under the following assumptions:

1. It is based on a wide range of experimental data with uncertainty values of +0.03 to +0.05% in the density values.
2. It is valid for a wide range of pressure and temperature values, even beyond the triple (critical) point in the phase-diagram of CO_2.
3. The EOS can be extrapolated up to the limits of the chemical stability of CO_2.

The only limitation of this EOS is that it is time-expensive to evaluate in dynamic numerical simulations because it consists of a large number of algorithms and exponentials.

The phase equilibria calculations in STOMP-CO_2 code [42] are conducted via a couple of formulations by Spycher et al. [47] and Spycher and Preuess [48] that are based on Redlich–Kwong equation of state with fitted experimental data for water–CO_2 flow systems. The mole fraction of water in the gas phase ($X_g^{H_{2o}}$) and mole fraction of the CO_2 in the aqueous phase ($X_l^{CO_2}$) are calculated by the following equations:

$$X_g^{H_{2o}} = \frac{(1-B)}{\left(\frac{1}{A} - B\right)} \tag{5}$$

$$X_l^{CO_2} = B\left(1 - X_g^{H_{2o}}\right) \tag{6}$$

where:

$$A = \frac{K^0_{H_{2o}}}{\varnothing_{H_{2o}P}} exp\left[\frac{(P-P)\overline{V}_{H_{2o}}}{RT(K)}\right] \tag{7}$$

$$B = \frac{\varnothing_{CO_{2o}P}}{(10^3/M^{H_{2o}})K^0_{CO_2}} exp\left[-\frac{\left(P-P^0\right)\overline{V}_{CO_2}}{RT(K)}\right] \tag{8}$$

In Equations (7) and (8), K^0 is the thermodynamic equilibrium constant for water or CO_2 at temperature T in Kelvin (K), and reference pressure $P^0 = 1$ bar, P is the total pressure, $\overline{V}$ represents the average partial molar volume of each pure condensed phase, ϕ is the fugacity coefficient of each component in the CO_2-rich phase and R is the gas constant [42].

The aqueous saturation (S_w) is calculated by Van Genuchten [49] formulation that correlates to the capillary pressure (P_c) to the effective saturation (S_e):

$$S_e = \frac{S_w - S_{wr}}{1 - S_{wr}} = \left[1 + (\alpha \cdot P_c)^n\right]^m; \text{ for } P_c > 0 \tag{9}$$

where S_{wr} is the water residual saturation and α, n and m are the Van Gunechten parameters that describe the characteristics of the porous media.

During the injection period (drainage process), there is no gas entrapment because it only occurs during the imbibition process when the displaced water invades the domain back as soon as CO_2 injection stops leaving some traces of it trapped behind in some small-sized pores. As a result, the injected CO_2 can either exist as free or trapped gas.

The effective trapped gas is computed using a model developed by Kaluarachchi and Parker [50]:

$$\hat{S}_{gt}^{potential} = \left[\frac{1-\hat{S}_l^{min}}{1-R\left(\hat{S}_l^{min}\right)}\right] \tag{10}$$

where $\hat{S}_l^{min}$ is the minimum aqueous saturation (irreducible water saturation) and R is the Land's parameter [51] which relates to the maximum trapped gas saturation:

$$R = \frac{1}{\hat{S}_{gt}^{max}} - 1 \tag{11}$$

$\hat{S}_{gt}^{max}$ is the maximum trapped gas saturation that can be achieved during the drainage process. Maximum trapped gas and minimum aqueous (irreducible water) saturation are calculated by the following correlations by Holts [43]:

$$S_{gr}^{max} = 0.5473 - 0.969\,\phi \tag{12}$$

$$S_{wirr} = 5.6709\left[\log\frac{(k)}{\phi}\right]^{-1.6349} \tag{13}$$

where ϕ and k are the porosity and intrinsic permeability of the medium, respectively. The aqueous and gas relative permeabilities are computed by Mualem [52] correlation in combination with Van Genuchten [49] formulations, according to the following Equations (14) and (15), respectively:

$$k_{rl} = \left(\overline{S}_l\right)^{\frac{1}{2}}\left[1-\left(1-\left(1-\left(\overline{S}_l\right)^{\frac{1}{m}}\right)^{m}\right)\right]^2 \tag{14}$$

$$k_{rg} = \left(1-S_l\right)^{\frac{1}{2}}\left[1-\left(1-\left(1-\left(S_l\right)^{\frac{1}{m}}\right)^{m}\right)\right]^2 \tag{15}$$

where m is the pore distribution index, $\overline{S}_l$ is the effective aqueous saturation, which is calculated from Equation (4) and S_l represents the apparent aqueous saturation which is defined as the sum of the effective aqueous and entrapped CO_2 saturations [53].

2.2. Initial and Boundary Conditions

Three types of simulated domains—namely, homogeneous, uniform heterogeneous and non-uniform heterogeneous—were modelled in this study. They were assumed to be isotropic for most simulation runs and isothermal under a hydrostatic pressure gradient of 10.012 KPa/m with an open boundary condition, leading to scattered pressure build-up. The models were presumed to have no heterogeneity in the azimuthal direction, but different vertical-to-horizontal permeability ratios were studied, in some specific cases, to investigate the effect of anisotropy on the storage capacity and efficiency. The system was modelled as a 3D cylindrical domain and the results were compared to those when the system was considered as a two-dimensional radial flow to save computational time and requirements. The gravity and inertial effects were neglected.

Prior to injecting $ScrCO_2$ into the centre of the domain, it was considered to be fully saturated with brine with initial conditions, as illustrated in Tables 1 and 2. $ScrCO_2$ was injected through four grid-cells at the bottom layer of the grid for 30 years, followed by a lockup period of 4970 years. No flux

boundary condition was considered for the aqueous wetting phase (brine) at the injection well case as a west boundary, whilst the east boundary was set to be infinite with zero flux for CO_2 as a non-wetting gas phase. Zero flux was also considered at the top and bottom confining layers, forcing the injected CO_2 to swell crossways.

As an open storage system, the pressure build-up was not considered to be a limiting factor; however, the value of the maximum bottom-hole pressure at the injection well and hydrological effect on shallow groundwater sources had to be taken into consideration [23,54]. The injection rate for this simulation system was set according to the rock fracture pressure (P_{frac}) using the simplified model adopted by Szulczewski et al. [55], which calculates the pressure-limited storage capacity by:

$$M_p = 2\rho_{CO_2} HW \sqrt{\frac{kC}{\mu_b T}} \frac{P_{frac}}{\hat{p}_{max}} \tag{16}$$

where ρ_{CO_2} is the density of the injected gas, H and W are the height and width of the domain, respectively, k represents the intrinsic permeability, and C is the compressibility of the formation; μ_b is the bulk viscosity and P_{frac} is the fracture pressure.

For infinite aquifer, the value of the maximum dimensionless pressure ($\hat{p}_{max}$) in Equation (16) was ~0.87, according to Szulczewski et al. [55].

All parameters in Equation (16) were known, except for the fracture pressure of the rock, which can be defined as the effective vertical stress for deep aquifers and is determined by the following equation, given by Szulczewski et al. [56]:

$$\sigma'_v = (\rho_b - \rho_w)Z \tag{17}$$

where ρ_b, ρ_w represent bulk and brine densities, respectively, and Z is the depth at which the aquifer is located.

$$\rho_b = \rho_r \phi \tag{18}$$

where ρ_r is the rock density and $\varnothing$ is the formation porosity.

From Equations (16)–(18), the value of the injection rate for the model is set at 32 kg/s, which, according to Equation (16), results in a pressure build-up value of less than 1.5 magnitudes of the hydrostatic pressure. This value is far away from the average default values of the sustainable pressure (181% of the hydrostatic pressure gradient) reported for Dundee Limestone in the Michigan Basin in the USA, which is located at a 1200 m depth [23].

2.3. Storage Efficiency Calculation

Theoretically, the CO_2 sequestration efficiency in saline aquifers can be assessed by calculating the efficiency storage factor, which refers to the volume fraction of the pores occupied by the injected CO_2:

$$E_{aq} = \frac{V_{CO_2}}{V_\varnothing} \tag{19}$$

V_{CO_2} is the volume of injected CO_2, which can be calculated from the known mass rate of the injected gas under the hydrostatic conditions of the geological formation. $V_\varnothing$ is the volume of the pores in the domain:

$$V_\varnothing = V_t \phi_t \tag{20}$$

where V_t and $\varnothing_t$ are the total volume and total porosity of the domain, respectively.

To calculate the storage capacity in this research work, the modern equation, developed by Szulczewiski [34], was employed:

$$E_{aq} = \frac{G_{CO_2}}{\rho_g L_t WH\varnothing(1 - S_{wc})} \tag{21}$$

where G_{CO_2} is the total mass of the integrated CO_2 (dissolved and residually trapped), ρ_g is the density of CO_2 at hydrostatic conditions and W, L_t *and* H represent the width, total length and net thickness of the aquifer, respectively. $\varnothing$ defines the porosity of the rock and S_{wc} defines the connate (irreducible) water saturation.

This methodology has been implemented because it accounts for the net thickness of the aquifer rather than the whole thickness. This can be justified by the fact that only the higher permeability layers are targeted by the injected gas [34].

This study aims to investigate the impact of heterogeneity, permeability, grid resolution and injection methodology on CO_2-water system mobility and the behaviour of the injected scrCO_2 at different time steps on the CO_2 storage capacity and efficiency at a field-scaled domain. An archetype of actual field heterogeneity has been developed in a domain that consists of three stratums of sands intermingled with two layers of low permeability shales, as illustrated in Figure 1. All petrophysical and simulation parameters are shown in Tables 1 and 2, respectively.

A series of simulation cases (presented in Table 3) were setup to demonstrate different models of a computational domain, including homogeneous, uniform and non-uniform heterogeneous models with coarse and fine grid resolutions. The simulation runs comprised two different employed schemes of injection (continuous and cyclic). The continuous injection scheme involved 30 years of continuous injection at a constant rate of 32 kg/s (about 1 million metric tons (MMT) per year) while in the second scenario, the injection period was implicated in three cycles of 10 years, separated by two stopping periods of 5 years in between in order to ensure that the structural trapping mechanism ended and other trapping mechanism took their role before injecting a new cycle. Furthermore, three cases with different values of vertical-to-horizontal permeability ratio (k_v/k_h) were developed along with other models to assess the influence of injection scope and orientation of the injection well on the flow behaviour and CO_2 sequestration efficiency. In all 14 cases, the total simulation time was 5000 years, including injection and pausing times. This value was set up after many trial simulations to detect the steady state time scales. Before 1000 years, most of the injected gas would be in a free gas phase, which is subject to escape through any existing cracks or faults in the caprock. As the permanent sequestration of the injected CO_2 is the focus of this work, a new term of permanent sequestration factor of the aquifer (E_{aq}^{perm}) was introduced. This factor was calculated from the numerical simulation results by STOMP-CO_2 code [42] and compared for different cases under different conditions through various time scales.

Due to the density difference between the injected supercritical CO_2 (scCO_2) (about 280 kg/m^3) and the existing brine (about 1100 kg/m^3) (i.e., gravity driving forces), initially the former fluid percolates upwards to be physically trapped under the upper impervious layer (caprock). During this time, part of the gas dissolves in the existing brine to form an aqueous phase rich in CO_2, which is heavier than the ambient liquid and hence sinks down to settle at the bottom of the aquifer. As soon as the injection stops, the replaced brine invades the domain to reinstate the CO_2, leaving some traces of it behind in some small-sized pores in a process called residual or capillary trapping. These amounts of CO_2 are determined by the simulation code for different cases and utilized to calculate the capacity and efficiency of the simulated aquifer. The latter values are used to calculate the sequestration efficiency by:

$$\text{Total integrated } CO_2 \;=\; \text{Integrated aqueous } CO_2 \left(CO_2^{aq}\right) \;+\; \text{Integrated gas } CO_2 \left(CO_2^{g}\right) \tag{22}$$

$$\text{Integrated gas } CO_2^{g} = \;\text{Trapped gas } CO_2 \;(CO_2^{gt}) + \text{Free gas } CO_2 \left(CO_2^{gf}\right) \tag{23}$$

$$E_{aq}^{perm} = \frac{CO_2^{aq} + (CO_2^{gt})}{\rho_g L_t W H \varnothing (1 - S_{wc})} \tag{24}$$

where all parameters are explained in Equation (21).

Table 3. Simulation cases and conditions.

Case No.	Domain	Heterogeneity and Layers Thickness	Grid Resolution	Nodes Distribution (r, θ, z)	Permeability Ratio (k_v/k_h)	Injection Scheme (30 years)
Base-3D	Homogeneous	N/A 1 × 96 m	Coarse	(75, 4, 24)	1	Vertical continuous into lower section
Base-2D	Homogeneous	N/A 1 × 96 m	Coarse	(75, 1, 24)	1	Vertical continuous into lower section
1	Homogeneous	N/A 1 × 96 m	Coarse	(88, 1, 24)	1	Vertical continuous into lower section
2	Heterogeneous	Uniform 3 × 30 m, 2 × 3 m	Coarse	(88, 1, 24)	1	Vertical continuous into lower section
3	Heterogeneous	Non-uniform 3 × 30 m 2× variable	Coarse	(88, 1, 24)	1	Vertical continuous into lower section
4	Heterogeneous	Non-uniform 3 × 30 m, 2× var.	Coarse	(88, 1, 24)	1	Vertical batch * (10-5-10-5-10) into lower section
5	Homogeneous	N/A 3 × 30 m 2× variable	Coarse	(88, 1, 24)	1	Vertical batch * (10-5-10-5-10) into lower section
6	Homogeneous	N/A 3 × 30 m, 2× var.	Fine (+100%)	(176, 1, 48)	1	Vertical continuous into lower section
7	Homogeneous	N/A 3 × 30 m 2× variable	Coarse	(88, 1, 24)	1	Vertical continuous into lower section
8	Homogeneous	N/A 3 × 30 m 2× variable	Coarse	(88, 1, 24)	1	Vertical continuous Whole thickness
9	Homogeneous	N/A 3 × 30 m 2× variable	Coarse	(88, 1, 24)	0.1	Vertical continuous into the whole thickness
10	Homogeneous	N/A 3 × 30 m 2× variable	Coarse	(88, 1, 24)	0.01	Vertical continuous whole thickness 96 m **
11	Homogeneous	N/A 3 × 30 m 2× variable	Coarse	(88, 1, 24)	0.01	Horizontal continuous 96 m **
12	Homogeneous	N/A 3 × 30 m 2× variable	Coarse	(88, 1, 24)	0.01	Horizontal continuous 192 m **

* Batch injection schemes refer to the years of (injection–stop–injection–stop–injection). ** Width of the injection well maintaining constant injection rate.

Because the system was assumed to be boundless (open boundary conditions) with no pressure build-up, most of the integrated free gas was subject to migration away from the injection well along the overlapping layer and a small amount of it may sweep out of the domain through any existing fractures or faults in the overlaying caprock. Therefore, in this work the focus was on the storage efficiency of the aquifer in terms of the permanent sequestration of the injected CO_2, which occurs mainly through solubility and residual trapping mechanisms due to the insignificant influence of the mineral trapping mechanism for a few thousand years, according to De Silva et al. [39].

3. Results and Discussion

Injecting $scCO_2$ into a brine-saturated porous formation produces spatial distribution maps of both fluids. Figure 2 illustrates the integrated gas saturation maps and spatial distribution of the aqueous CO_2 mass fraction within the 3D cylindrical model of the simulated domain (case Base-3D in Table 3) at different time scales. It is shown that, soon after injection, the gas bounces upwards due to the density difference between the two fluids and simultaneously migrates crossways due to the pressure gradient between the injected $ScrCO_2$ and the in situ hydrostatic pressure. During this drift, some of the injected gas disperses into the existed brine, producing a CO_2-saturated aqueous phase that is heavier than the pure brine and, consequently, tends to sink down towards the bottom of the domain, forming a fingered structure, as displayed in Figure 2 (right).

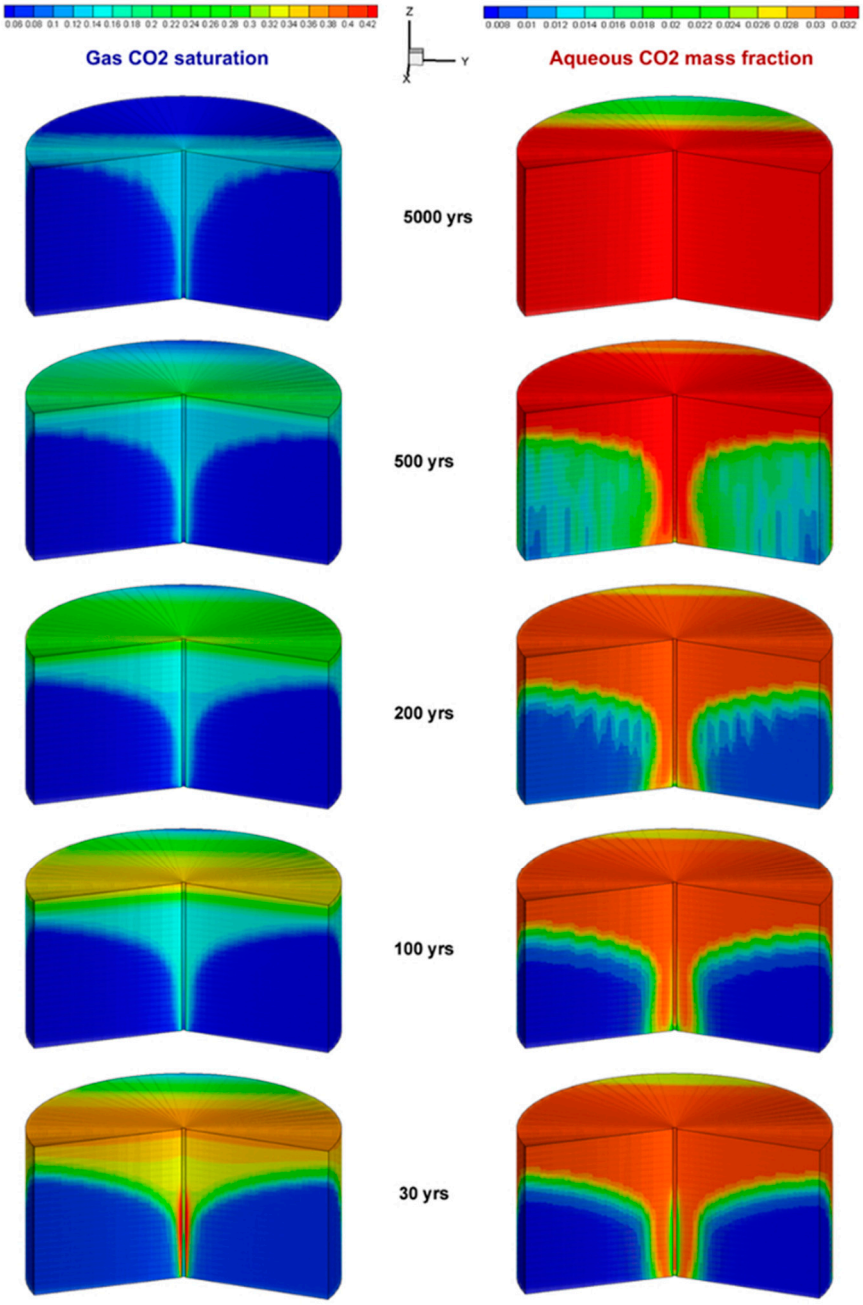

Figure 2. Free gas saturation and aqueous (dissolved) CO_2 mass fraction contours for a 3D homogeneous model at different time steps (case Base-3D in Table 1).

3.1. CO_2 Mobility and Behaviour

Due to the density difference between the injected gas and the hosted brine, the buoyancy forces initially dominate the water–CO_2 flow system. The injected scrCO_2 displaces the existing brine soon after the injection starts, and the gas moves upwards to be physically trapped under the overlaying impermeable layer (caprock). The flow system involves interfacial contact between the two fluids that results in considerable amounts of the free CO_2 gas to dissolve in the accommodated brine representing the solubility trapping mechanism. This is in addition to the amount of the gas that is trapped because of the capillarity and interfacial forces between the pore surface and the percolating gas.

Simultaneously, limited traces of CO_2 trapped in the locale (space) even during the injection lifetime due to the injection pressure that forces some drops of the gas into some small-sized pores.

However, these amounts are insignificant and further subject to be snapped off by the invading brine during imbibition. The actual capillary trapping is noticeable only after the gas injection stops. As soon as the injection ceases after 30 years, the residual trapping mechanism dominates when the replaced brine invades back the domain to sweep the integrated gas out of the pores. During this process, traces of CO_2 get detached from the trailing part of the gas plume and pierce into the small-sized pores due to the capillary forces.

The displayed trends in Figure 3A exhibit that, after 100 years, ~74% of the injected scrCO_2 was structurally trapped as a free integrated gas in the homogeneous domain. ~17.5% of the injected CO_2 was dissolved in brine and the remaining 8% was residually trapped in small-sized pores due to the capillarity. For the heterogeneous model in Figure 3B, on the other hand, it was observed that ~70% of the injected gas was trapped as a free gas, 20.49% was dissolved in the brine, while 9.4% was disconnected from the plume trailing edge and adhered to the rock surface inside some small-sized pores, due to the surface tension forces.

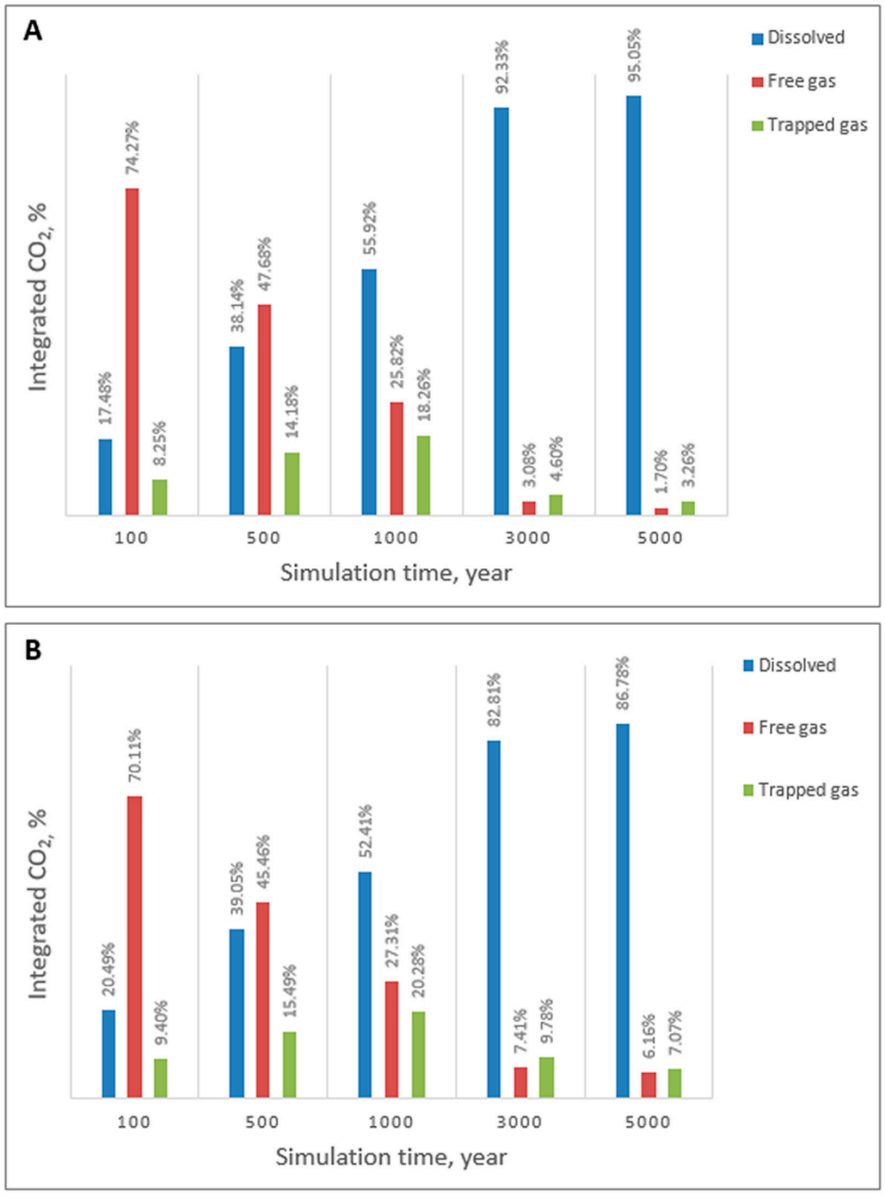

Figure 3. Various phases of integrated CO_2 trends in: (**A**) homogeneous porous domain (case 1); (**B**) uniform heterogeneous domain (case 2) in Table 3.

The findings from this study have shown that, under similar hydrostatic conditions and petrophysical characteristics, homogeneous formations promote more CO_2 dissolution, owing to the fact that, under the same hydraulic gradient, fluid flows faster in homogeneous porous media compared to that in the heterogeneous porous medium, which limits fluid seepage and is consistent with some previously published studies [57,58].

This fast migration induces more contact with fresh brine, leading to the higher dissolution rates of CO_2. This can be seen in Figure 3A,B, which shows that only 1.7% of the injected CO_2 was left as a free gas in the homogeneous model at the end of the simulation compared to the heterogeneous case, in which more than 6% of free gas was recorded.

The timing maps of CO_2 sequestration by each trapping mechanism are depicted in Figure 3 for homogeneous and heterogeneous formations. It can be seen from the figure that, during the first few hundreds of years, the structural trapping mechanism dominates (i.e., more free CO_2 gas) while, after thousands of years, the solubility trapping becomes the dominant mechanism (i.e., more CO_2 dissolves in the brine). The maximum amount of CO_2 is residually trapped at about 1000 years and declines later because some of it dissolves into the surrounding brine to form weak carbonic acid that reacts with the rock material and precipitates as solid carbonates after a few thousand years.

3.2. Impact of Heterogeneity

To investigate the impact of different types of heterogeneity (uniform and non-uniform) on the propagation of CO_2 profiles, P_c-S_w relationships and storage efficiency, three numerical cases—namely 1, 2 and 3—with their employed conditions, illustrated in Table 3, have been implemented in this study. It is a fact that the permeability of geological formations is strongly dependent on their porosity and heterogeneity, and it plays a key role in understanding water–CO_2 flow in the subsurface. This influence is clearly exposed in Figure 4, which demonstrates different maps of gas distribution in the modelled domains.

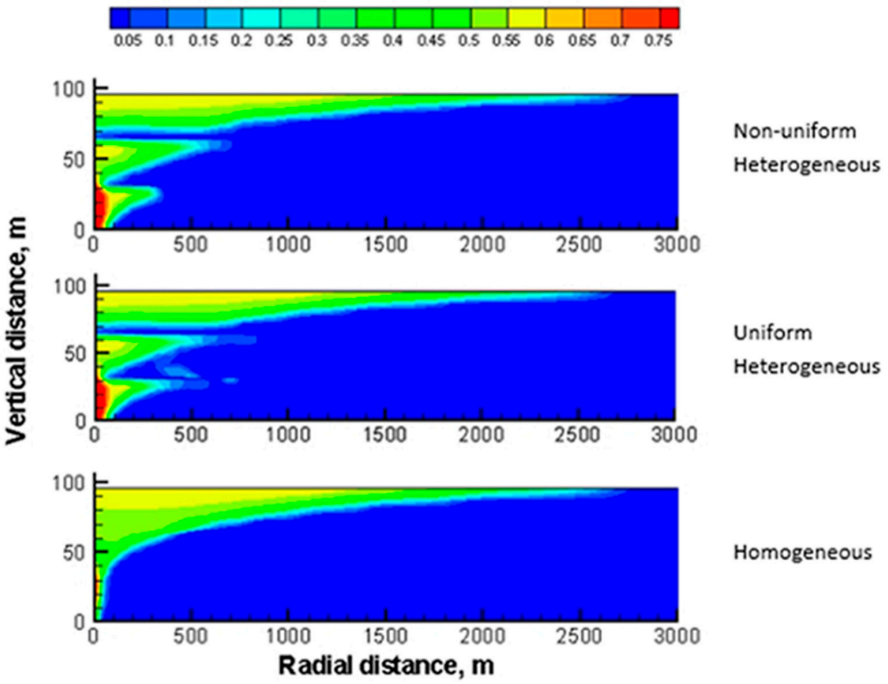

Figure 4. Spatial distribution of CO_2 after 30 years of simulation (end of injection) for homogeneous media (case 1) and heterogeneous media (cases 2 and 3) in Table 3.

The achieved maps depict that the homogeneous domain has produced sharp-edged contours, while the heterogeneous media resulted in irregular edges exposing more contact surface area between

the CO_2 and the local brine, which enhances the storage efficiency. The irregular frontages in the heterogeneous media are due to the intermingled layers of shale that restrict the injected gas from moving across different layers of the domain that results in less contact with the ambient brine and less subjectivity to entrapment in more small-sized pores. Heterogeneity is found to have a substantial impact on the amounts of trapped and dissolved gases, as a result of the influence on the capillary pressure–saturation relationship, which is imitated by an increase in the amount of the residually trapped CO_2.

Figure 5A shows that, soon after gas injection stops (i.e., imbibition process starts), the amount of the trapped gas sharply increases when the replaced brine invades back into the domain and isolates some blobs of CO_2 from the trailing edge of the mobile CO_2 plume. After 200 years, this progress slightly retards because part of the trapped gas tends to dissolve in the brine. This increase continues until 1400 years of simulation, when the trapped gas profiles steeply decline before tending to settle after 3000 years. The figure further demonstrates more residually trapped gas in the heterogeneous models compared to the homogeneous ones at the end of the simulation.

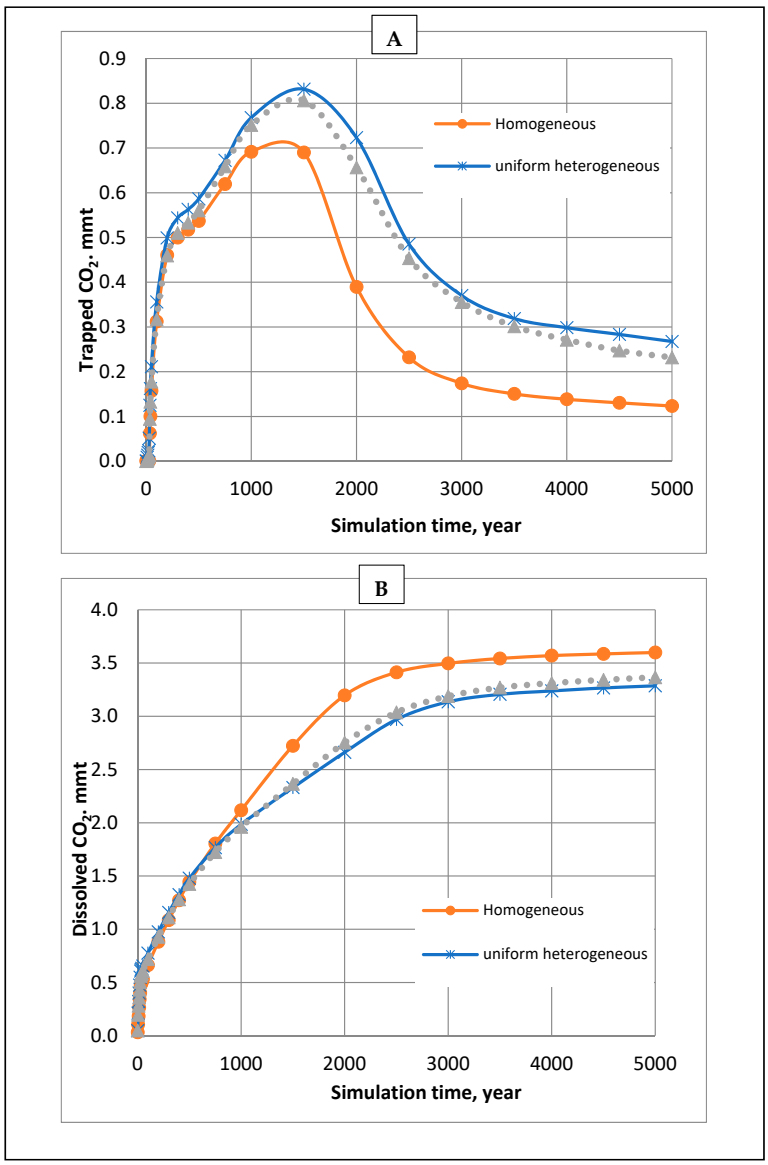

Figure 5. Effect of heterogeneity for cases 1, 2 and 3 on (**A**) CO_2 residual trapping and (**B**) dissolved CO_2.

In Figure 5B, no effect of heterogeneity on CO_2 solubility was detected before 800 years of simulation because the system was totally dominated by buoyancy and hydrostatic forces. Afterwards, it was observed that more CO_2 got dissolved in the homogeneous domain compared to both types of heterogeneous ones by about 17% after 2000 years. However, this influence approximately declined after 4000 years to 9%. It is apparent from the results, displayed in Figure 5B, that both types of heterogeneity provide almost identical but lower amounts of dissolved CO_2 compared to the homogeneous media throughout the simulation time. This suggests that gas migration is more straightforward through homogeneous media, owing to the lesser resistance to flow.

In contrast to the results by Chasset et al. [35], the increase in CO_2 dissolution can be justified by the presence of intermingled layers of shale that play a role as internal barriers to retard the vertical migration and the promote lateral flow of the injected CO_2. However, this horizontal movement retards after the injection period due to the limited hydraulic gradient, which limits gas contact with more fresh brine, leading to a reduction in gas assimilation and dissolution. The values of trapped and dissolved CO_2 surely affect the storage capacity of the site; however, this impact is applicable to a very limited extent in agreement with the results from a recent study by Zhao et al. [58], which revealed that strong heterogeneity in geological formations reduces the storage capacity because it limits gas seepage.

In spite of the two contrary trends, Figure 6, shows that heterogeneous domains are more efficient in storing the disposed gas by a factor of about 15% compared to the homogeneous ones under similar conditions. This does not comply with the numerical results depicted in Figure 3, that show higher values of free-gas CO_2 left off by the end of simulation in the homogenous domain compared to the heterogeneous one. This controversy is due to the net thickness parameter suggested by Szulczewski [34] for Equation (21) instead of the total thickness of the modelled domain. To implement this in our calculations, the thicknesses of the shale layers were excluded and this resulted in less values of the net thickness in cases 2 and 3 (see Table 3), leading to smaller pore volume available to store the injected CO_2 and, consequently, higher values of storage efficiency were achieved for the heterogeneous domains using Equation (21). This is an important point that needs further investigation to assess the effectiveness of this method to more accurately determine the storage efficiency in open-boundary domains.

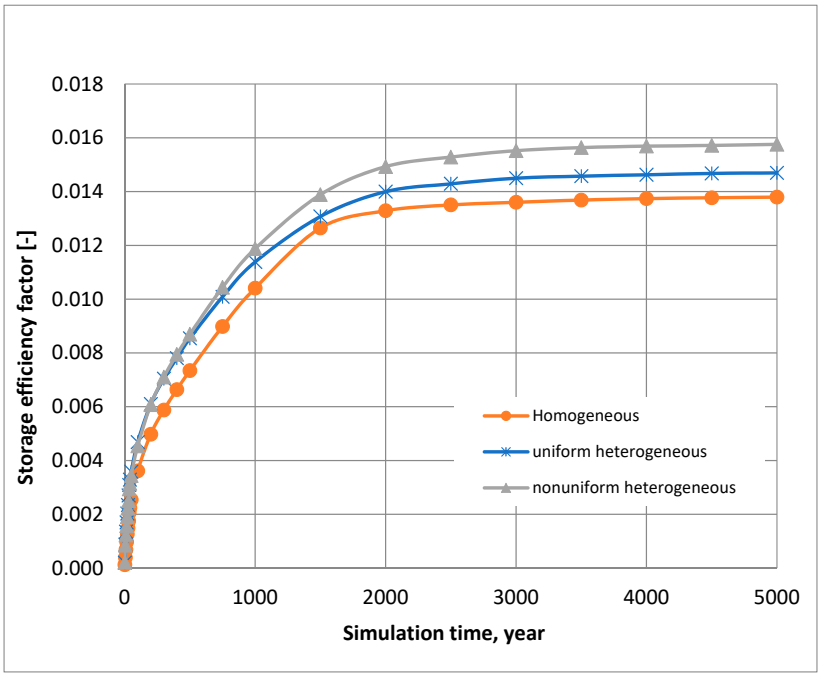

Figure 6. Influence of heterogeneity on storage efficiency factor for Cases 1, 2 and 3 (Table 3).

3.3. Effects of Cyclic Injection on CO_2 Mobility and Sequestration

Saturation (S_w)—relative permeability (k_r) relationship is a key feature that describes the CO_2–water flow system because it has a huge influence on the behaviour and fate of the injected gas in the subsurface. This study has investigated the impact of the injection methodology on the S_w-k_r relationships and eventually on the effectiveness of the disposed gas storage. Purposely, an observation point was setup at 200 m radially away from the injection well (to avoid the effect of the high pressure difference forces close to the wellbore) and 15 m from the bottom of the aquifer, which represents the midpoint of the lower segment of the domain into which the gas injection takes place.

The achieved results from implementing cyclic injection techniques are demonstrated in Figure 7A, that manifests the development of gas relative permeability profiles for continuous and cyclic injection methods (see cases 3 and 4 in Table 3). The influence of the cyclic injection is obvious from the fluctuating profiles from which it can be observed that, for the continuous injection method, the relative permeability of the CO_2 curve declined from a peak value of (0.43) after 10 years to zero by the end of the injection period (30 years). The figure further displays the three cycles of injection impact on the permeability curves with highest peak values of 0.43, 0.66 and 0.7. This impact has been directly imitated on the gas saturation trends in Figure 7B, which evidences the favourite of cyclic injection method because higher amounts of injected CO_2 were found to be safely trapped after the cease of injection.

This is comparable to the continuous injection case, which depicts higher values of gas saturation after the end of injection; however, these values decline soon after that to reach a value of 0.01 after 2000 years of simulation (this is not shown in Figure 7B, which is magnified to show more details about the drainage period).

This variation can be justified by the two additional cycles of imbibition process that lead to more blobs of CO_2 getting disconnected from the trailing edge of the ascending gas plume.

For the homogeneous models (see cases 1 and 5 in Table 3), cyclic injection confirmed no effect on CO_2 dissolution and almost equal amounts of free gas were left off in the domain by the end of the simulation runs, as shown in Figure 8. However, for the heterogeneous domains (cases 3 and 4), continuous injection produced slightly greater profiles of CO_2 dissolution.

In contrast, the residual trapping of CO_2 in heterogeneous media was found to be more sensitive to the cyclic injection because the simulation results revealed that more CO_2 was trapped using the cyclic injection method in the heterogeneous modelled domain compared to the continuous one after 5000 years of simulation, as illustrated in Figure 8.

Table 4 concludes that cyclic injection into homogeneous domains increases the amount of trapped CO_2 gas to some extent (compare cases 1 and 5). However, continuous injection into heterogeneous formations enhances the storage efficiency factor (determined by Equation (21)) by about 0.0003, that represents 1.7% (compare cases 3 and 4), because it can be seen from the table that by applying continuous injection (case 3), 0.773 MMT (approximately 0.17%) more of the injected gas was permanently sequestered either by residual or solubility sequestration mechanism using continuous injection techniques.

In agreement with the results by Juanes et al. [59], this can be justified by the increase in capillary pressure which forces more CO_2 into smaller-sized pores to be trapped and exposed to dissolution in the brine at later stages of storage. In contrary for the cyclic injection, releasing pressure after 10 years encourages the gas plume to percolate upwards through larger pores to accumulate at the top of the domain as a free gas.

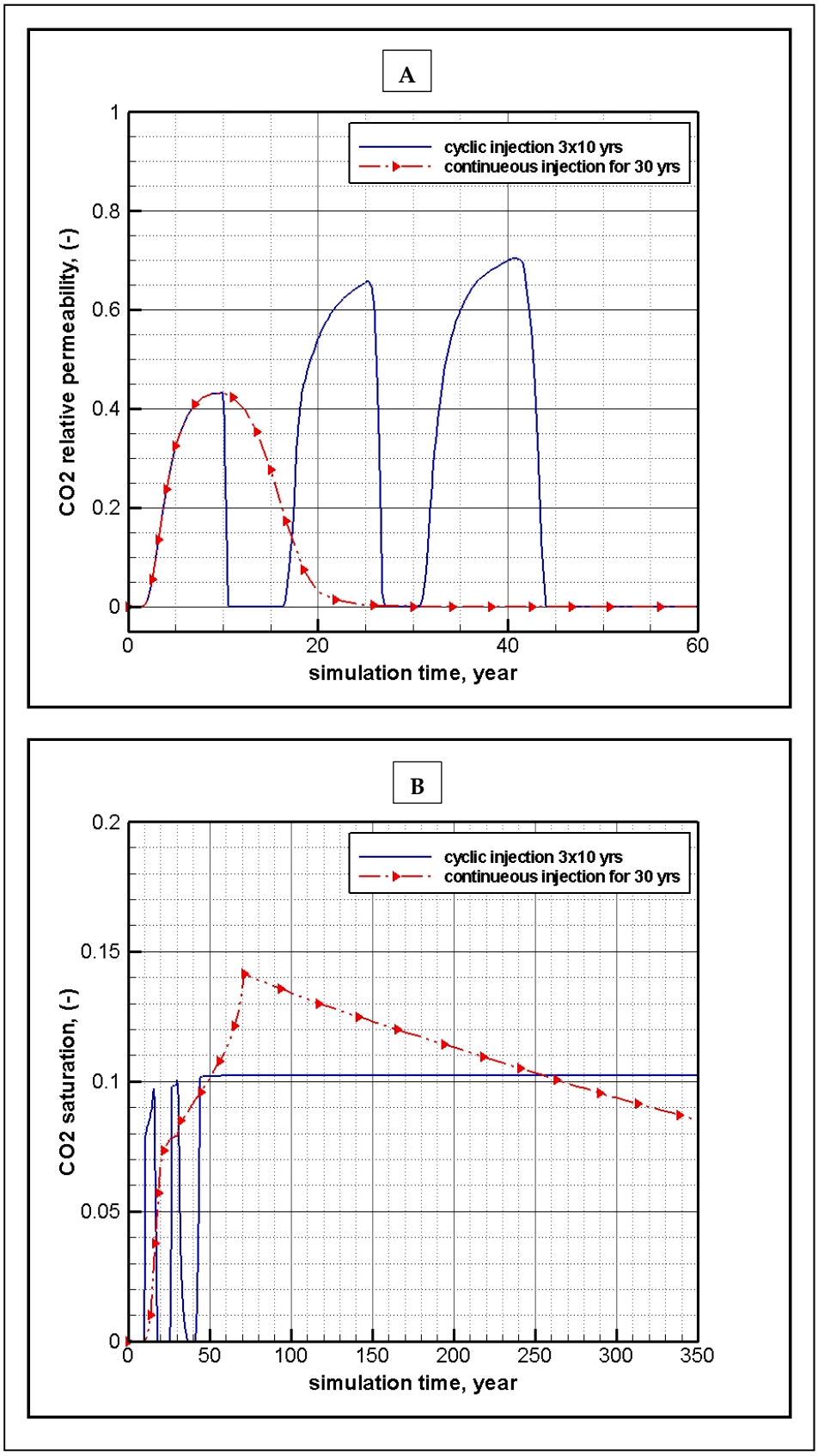

Figure 7. Impact of cyclic injection for cases 3 and 4 on: (**A**) CO_2 relative permeability; (**B**) CO_2 saturation.

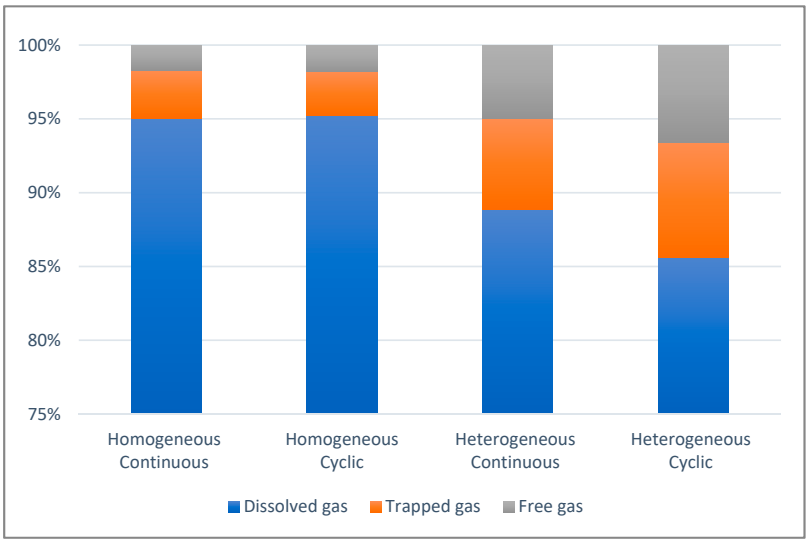

Figure 8. Impact of cyclic injection on different integrated CO_2 phases in DSAs for cases 1, 5, 3 and 4 in Table 3, respectively.

Table 4. Simulation results and calculated efficiency factor for all modelled cases.

Case No.	Description	Dissolved Gas MMT **	Trapped Gas MMT **	Free Gas MMT **	Storage Efficiency Factor [–]
Base	Homogeneous Isotropic Coarse grid, Cont. Vert. Inj. Into lower section	16.095	0.758	0.495	0.0372
1	Homogeneous Isotropic Coarse grid, Cyclic Vert. inj. Into lower section	28.800	0.986	0.513	0.01379
2	Homogeneous Anisotropic Coarse grid, Cont. Vert. inj. Into whole thickness	26.290	2.141	1.864	0.0417
3	Irregular Heterogeneous Isotropic Coarse grid Cont. Vert. inj., lower section	26.929	1.854	1.511	0.0158
4	Irregular Heterogeneous Isotropic Coarse grid Cyclic Vert. inj., lower section	25.941	2.355	1.999	0.0155
5	Homogeneous Isotropic Coarse grid, Cont. Vert. inj. Into lower section	28.858	0.886	0.551	0.0138
6	Homogeneous Isotropic Fine grid, Cont. Vert. Inj. Into lower section	29.161	0.637	0.497	0.0138
7	Homogeneous Isotropic Coarse grid, Cont. Vert. inj. Into lower section	28.147	1.282	0.866	0.0136
8	Homogeneous Isotropic Coarse grid, Cont. Vert. inj. Into whole thickness	28.241	1.217	0.838	0.0136
9	Regular Heterogeneous Isotropic Coarse grid Cont. Vert. inj., lower section	26.190	2.360	1.745	0.0132
10	Homogeneous Anisotropic Coarse grid, Cont. inj. Vertical inj. well 96 m	21.367	4.699	4.229	0.0121
11	Homogeneous Anisotropic Coarse grid, Cont. inj. Horizontal inj. well, 96 m *	18.787	6.977	4.532	0.0119
12	Homogeneous Anisotropic Coarse grid, Cont. inj. Horizontal inj. well 192 m *	19.885	5.167	5.244	0.0116

* Horizontal injection well at the bottom of the domain starting from the centre point. ** MMT = million metric ton (10^9 kg).

3.4. Effect of Vertical Injection

This section extends a previous work [9] to further optimize the vertical injection method with the aim to investigate the storage efficiency enhancement. To carry this out, two simulation cases were conducted, implementing two different scopes of vertical injection (see cases 7 and 8 in Table 3). In case 7, scrCO_2 was injected into the lower segment of the aquifer through four vertical grid cells of 4 m, while for case 8, the injection was executed over 24 blocks (i.e., over the whole thickness of the aquifer that extends to 96 m).

In terms of the dissolution of the injected scrCO_2, unexpectedly no significant effect was observed at all-time scales for case 7. On the other hand, slightly more trapped gas concentrations within the vicinity of the injection well were demonstrated for case 8, as shown in Figure 9. This is because, in this case, the whole amount of the gas was injected through the lower segment of the domain, most of which was influenced by the reversing brine tendency to disconnect more blobs of CO_2 from the rambling edge of the gas plume. In contrast, when the injection applied into the whole thickness of the domain (case 8), only a sixth of the scrCO_2 mass rate was injected into the lower section of the model and most of this amount had bounced upwards before the imbibition process started. This means that only a significantly small part of the injected gas was affected by the raiding brine, leading to a reduced amount of residually trapped gas. It is evidenced from the achieved results that injecting CO_2 through the whole thickness of the domain slightly reduced the amount of the free gas left within the domain in medium terms of storage by 0.028 MMT (about 3.2%) as depicted in Table 4 for cases 7 and 8. However, the injection scope has shown no sensible influence on the storage efficiency because both cases returned almost identical values of storage efficiency factor, as presented in Table 4.

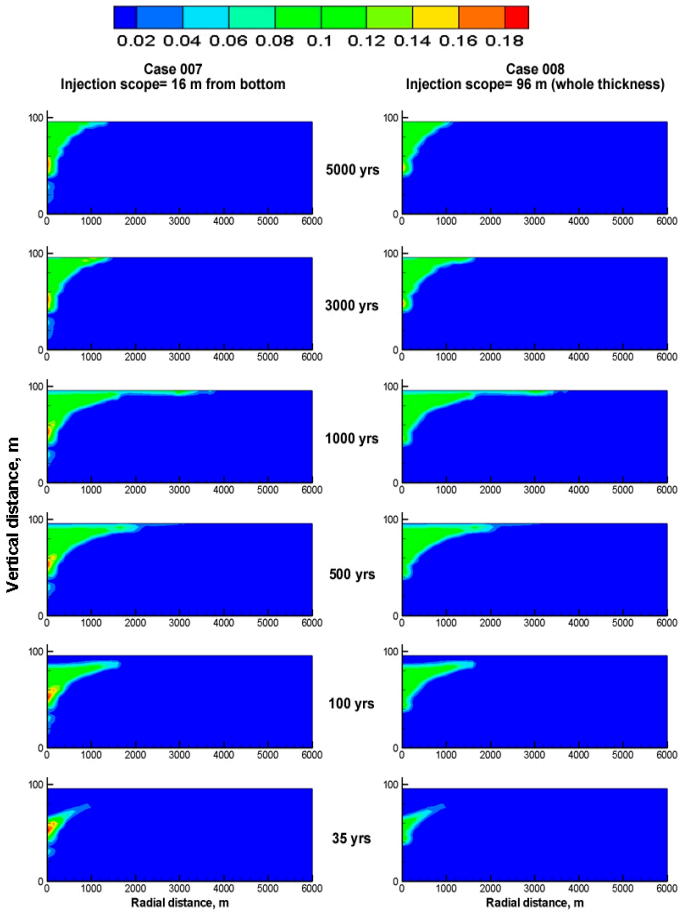

Figure 9. Impact of injection scope on trapped CO_2 mass distribution.

3.5. Impact of Directional Permeability Ratio

In the aim of assessing the effect of heterogeneity anisotropy in geological formations on the efficiency of storage, three models of a hypothetical aquifer with values of vertical-to-horizontal permeability ratios (k_v/k_h) equivalent to 1.0, 0.1 and 0.01 were developed and modelled (see cases 8, 9 and 10 in Table 3). This array was set up as a realistic figure for most sandstone rocks according to a relatively new study by Widarsono et al. [60].

The obtained results depicted in Figure 10, show the deceptive influence of the permeability ratio on the CO_2 plume shape and spatial distribution maps. While the plume tends to horizontally extend further along the overlaying layer at higher permeability ratios, more CO_2 shows the tendency to migrate laterally within the two lower layers of the domain for lower values of permeability ratio. This owes to the fact that lower permeability in the vertical direction restrains the upward movement of CO_2, forcing the injected gas to migrate horizontally across the domain, proposing more gas into small-sized pores where it is more likely to be permanently entrapped when the brine invades back into the domain after the injection stops, which is referred to as residual trapping.

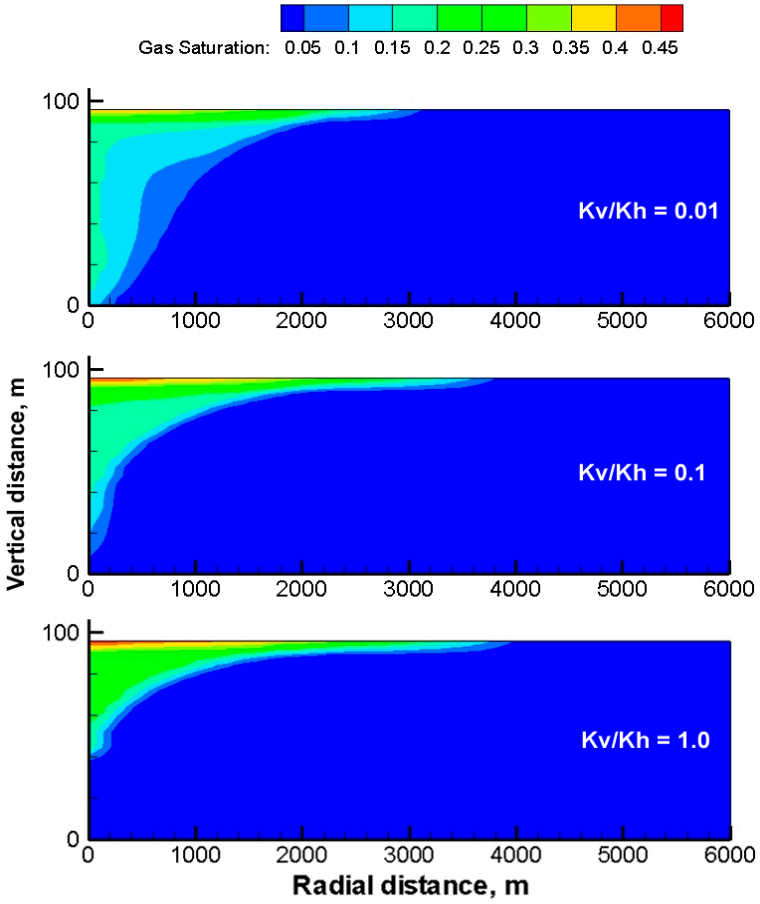

Figure 10. The impact of the vertical/horizontal permeability ratio on CO_2 distribution after 500 years in a homogeneous domain. Cases 8, 9 and 10 in Table 3.

The latter impact is evidenced in Figure 11A, which shows significantly greater amounts of trapped gas in cases of lower permeability ratios at all post injection time steps.

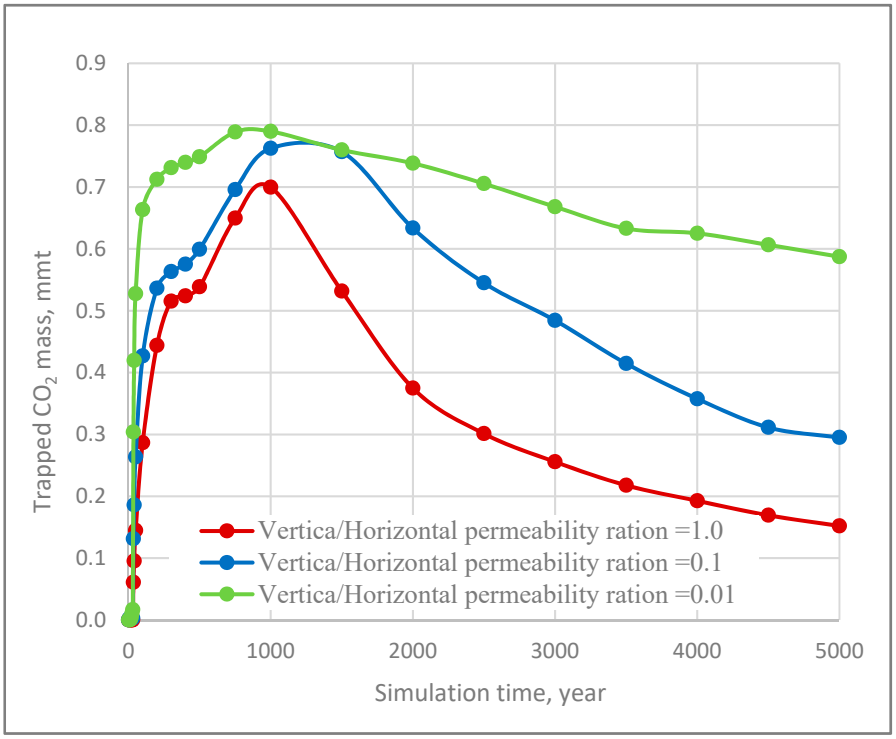

(**A**)

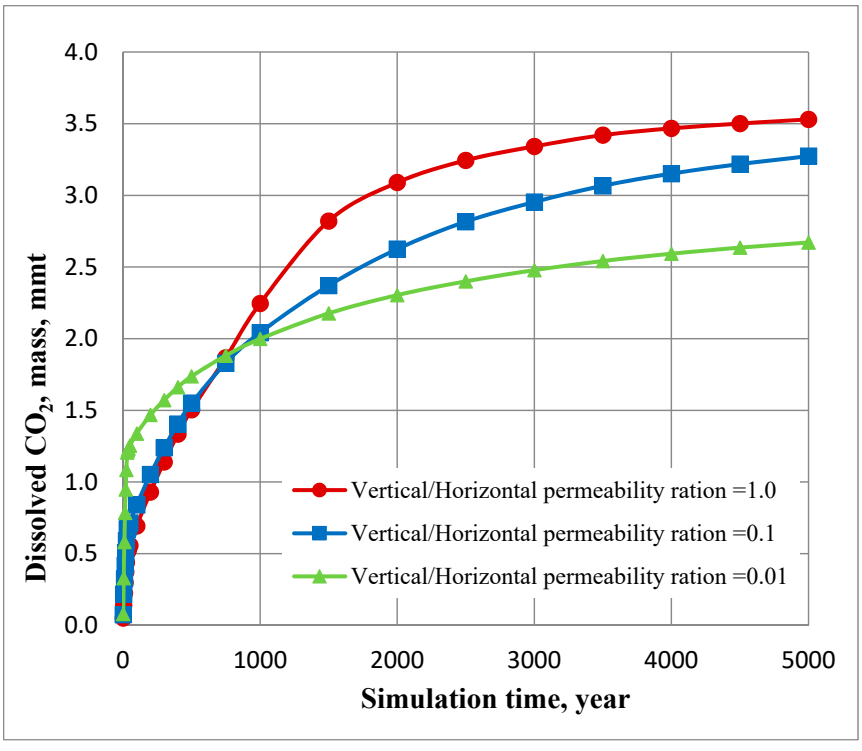

(**B**)

Figure 11. (**A**). Impact of vertical-to-horizontal permeability ratio on the integrated free CO_2 for cases 8, 9 and 10. (**B**). Impact of vertical-to-horizontal permeability ratio on dissolved CO_2 gas in a homogeneous domain for cases 8, 9 and 10 in Table 3.

One of the stupendous returns from this study is the inflection point in the gas dissolution trends after around 800 years of the simulation lifetime, as noticeable in Figure 11B. This deviation occurred because at early stages, the flow system was entirely dominated by the structural trapping mechanism, in which most of the injected gas remained in free phase. This mechanism is mainly dependent on the upwards movement of the free gas that is more effective at higher vertical permeability values (i.e., larger values of (k_v/k_h)), as explained previously in this section. The horizontal movement of the gas, due to the pressure gradient and low vertical permeability, promotes more contact between the two fluids, leading to more dissolution of CO_2 in the formation brine at early stages (solubility trapping). However, this migration has no significant impact compared to the large buoyancy forces at later stages.

This clarifies the larger amounts of dissolved CO_2 at lower values of k_v/k_h before 800 years in Figure 11B. By approaching 1000 years of simulation, the solubility trapping mechanism takes control because the density and pressure gradient driving forces decline when most of the integrated gas has either settled at the top of the domain or within the vicinity of the injection well, as illustrated in Figure 10 (see case 8 in Table 3). Consequently, the domain becomes dominated by the solubility trapping, which is based on the contact interfacial area between the two fluids and the hydrostatic conditions that influence the CO_2 dissolution rate in the surrounding brine. CO_2 dissolution into the formation brine creates a denser aqueous phase that tends to sink downwards when the vertical movement becomes important to maintain more gas contact with the fresh brine, leading to more dissolution of the gas into the brine. This convectional movement is easier at higher permeability ratios that result in larger amounts of gas dissolution.

Despite all this evidence, the determined storage efficiency for different permeability ratios using Equation (21) by Szulczewski [34] for open boundary domains has shown better storage efficiency at lower permeability ratios. This is significantly controversial and requires more investigation and discussion because our repeated numerical experiments have revealed contrasting results (see Figure 12A,B). This can be referred to as the length parameter used in Equation (21) to calculate the effective volume of the domain and, consequently, the CO_2 mass that can be stored. The author suggested using the maximum extent of the gas plume to calculate the effective volume; however, our simulation results revealed a huge difference in the obtained plume lengths for cases 8, 9 and 10 in Table 3. They were found to be 3965, 3802 and 3135 m for permeability ratios of 1.0, 0.1 and 0.01, respectively (see Figure 10).

This significant difference has returned unrealistic values of the storage efficiency when implemented in Equation (21), because looking at Figure 12A, it can be evidently noticed that higher permeability ratios produced greater amounts of dissolved and trapped CO_2, and less amounts of free-gas (i.e., enhanced solubility and residual trapping of the injected gas). It is apparent from the figure that, for k_v/k_h values of 1.0, 0.1 and 0.01, the achieved permanent trapping rates were 29.457 MMT (97%), 28.55 MMT (87%) and 26.066 MMT (71%), respectively.

Depending on the findings from this study, it is suggested that the plume length parameter in Equation (21) is reviewed and presented by a more realistic value to make the equation further applicable to various CO_2 injection scenarios into geological formations.

In this work, the total length of the domain, which extends far enough that the gas plume does not reach it, was used in order to avoid any boundary effects on the in situ pressure build-up or gas seepage from the computational domain for all simulation runs (i.e., to employ an open boundary condition away from the injection well). This means that the whole aquifer volume was used to calculate the storage efficiency factor, which explains the small-obtained values of the efficiency factors in Table 4. Using this total length in Equation (21) to determine the sequestration efficiency has returned more realistic values of the storage efficiency in terms of the directional permeability effect, as shown in Figure 12B, which indicates that the storage efficiency factor of any aquifer increases proportionally with the vertical-to-horizontal permeability ratio (see cases 8, 9 and 10 in Table 4).

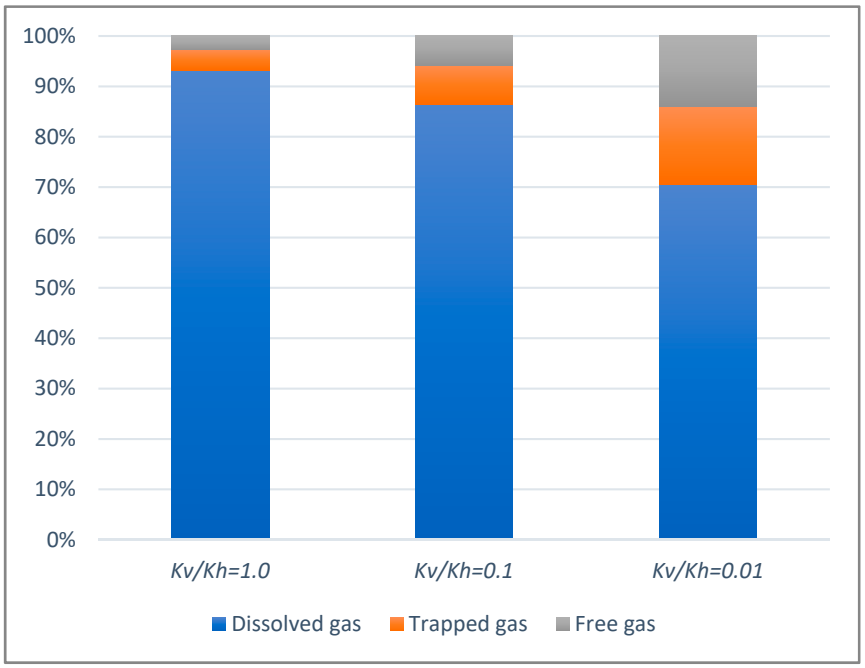

(**A**)

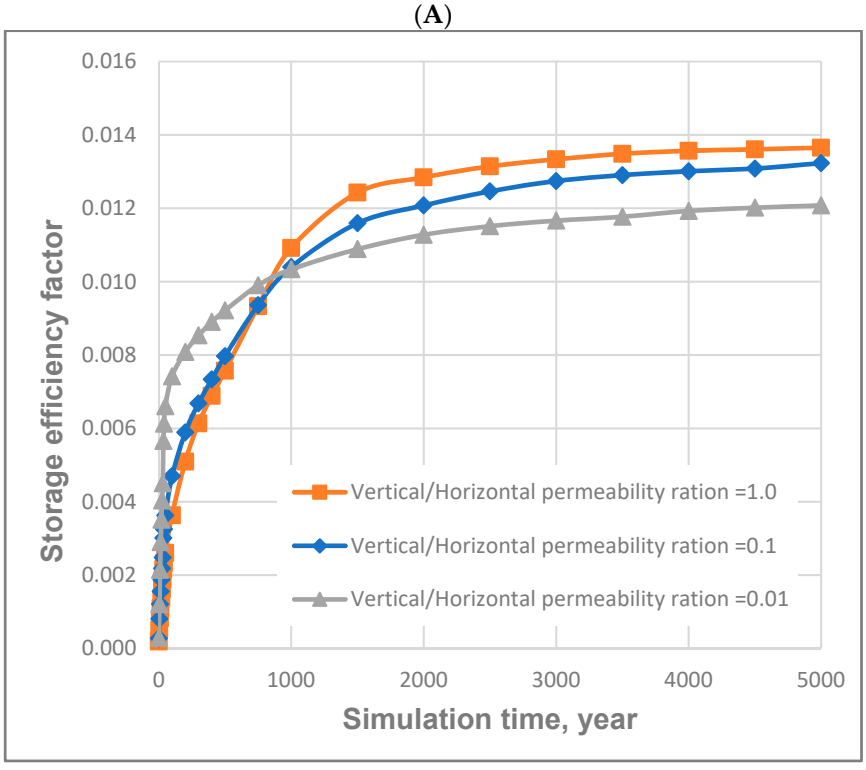

(**B**)

Figure 12. (**A**). CO_2 storage efficiency at different permeability ratios based on the numerical results plume length (see cases 8, 9 and 10 in Table 4). (**B**). CO_2 storage efficiency at different permeability ratios based on maximum plume length used in Equation (21) (see cases 8, 9 and 10 in Table 4).

3.6. Influence of Injection Orientation

Injecting CO_2 into sedimentary formations through horizontal wells has been a subject of many research works and review studies, most of which are based on applying horizontal injection into confined geological formations, considering the induced pressure build-up. While some authors

conclude that injecting CO_2 via horizontal injection wells improves the trapping efficiency [39], others find that such a methodology influences the mechanical stability of the overlaid caprock and does not improve the storage efficiency in the long term [40,61].

In this study, we investigated the influence of the injection orientation on the hydrodynamic behaviour of CO_2 and storage efficiency for an open boundary model and compared the results with those for the conventional vertical injection methodology. Purposely three simulation models were developed (see cases 10, 11 and 12 in Table 3) to identify the impact of the injection orientation on the storage efficiency and P_c-S_w relationship in geological formations. Both vertical and horizontal injection wells were set up for 96 m for cases 10 and 11, while the horizontal well length was extended to 192 m for case 12. All other simulation conditions were similar for the three cases and a constant injection rate was maintained to run the simulations over different well lengths (96 and 192 m).

The achieved numerical results revealed that injection orientation has a significant influence on the gas migration and behaviour in unconfined geological formations, as depicted in Figure 13, that highlights the disparity between the gas distribution contours achieved through using horizontal injection wells (cases 11 and 12 in Table 3) and those obtained from the vertical injection methodology (case 10).

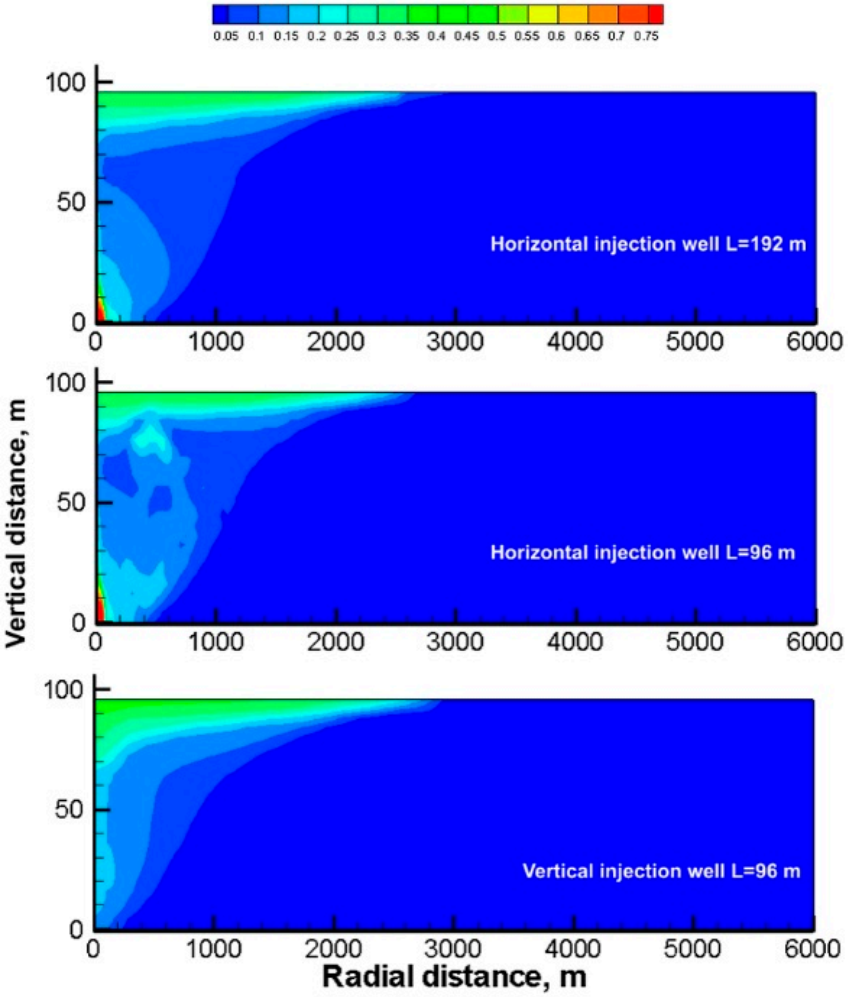

Figure 13. Integrated CO_2 distribution maps for different injection methods after 50 years in a homogeneous domain. Cases 10, 11 and 12 in Table 3.

The figure exhibits that a noticeable portion of the injected gas was trapped by the displacing brine in the case of the aquifer-thickness equivalent horizontal injection well (96 m) compared to the

longer horizontal well (192 m). This can be attributed to the large injection mass flow rate per unit area (i.e., limited number of gridlocks) which delayed the upwards propagation of the buoyant CO_2, leading to only part of it reaching the top of the domain to create a thin tongue-like shape that migrated crossways. The other portion of the injected gas was exposed to be encountered by the invading brine that physically isolated blobs of it within the local pores network to be dissolved at later stages.

Using horizontal injection techniques was found to increase the quantities of the trapped gas, as presented in Table 4, due to the magnified values of average capillary pressure. Unexpectedly, the amount of the trapped gas was found to be significantly less than that which was achieved by the shorter horizontal well. This can be explained by the smaller injection rate per unit area in the first case, which promotes more percolation of the free-gas towards the top of the aquifer, as shown in Table 4. Despite the relative increase in the gas dissolution depicted in Figure 14A, for the longer horizontal well, the amount of the free-gas left off by the end of the simulation was higher, as shown in Figure 14B, leading to lower storage efficiency, as evidenced in Figure 15.

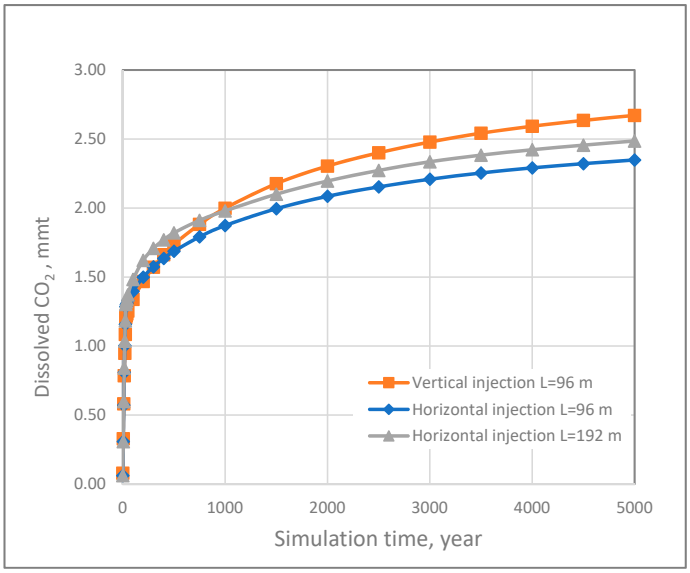

(A)

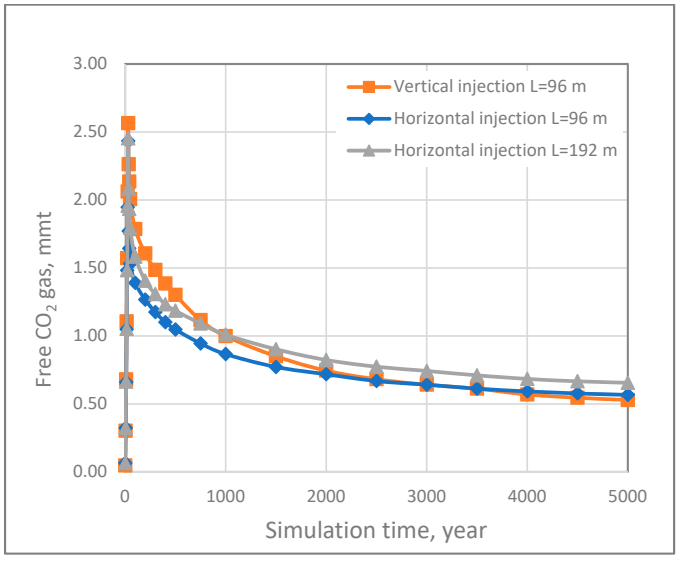

(B)

Figure 14. (**A**). Effect of injection orientation for cases 10, 11 and 12 (Table 3) on CO_2 solubility in a homogeneous domain. (**B**). Effect of injection orientation for cases 10, 11 and 12 (Table 3) on free-gas CO_2 in a homogeneous domain.

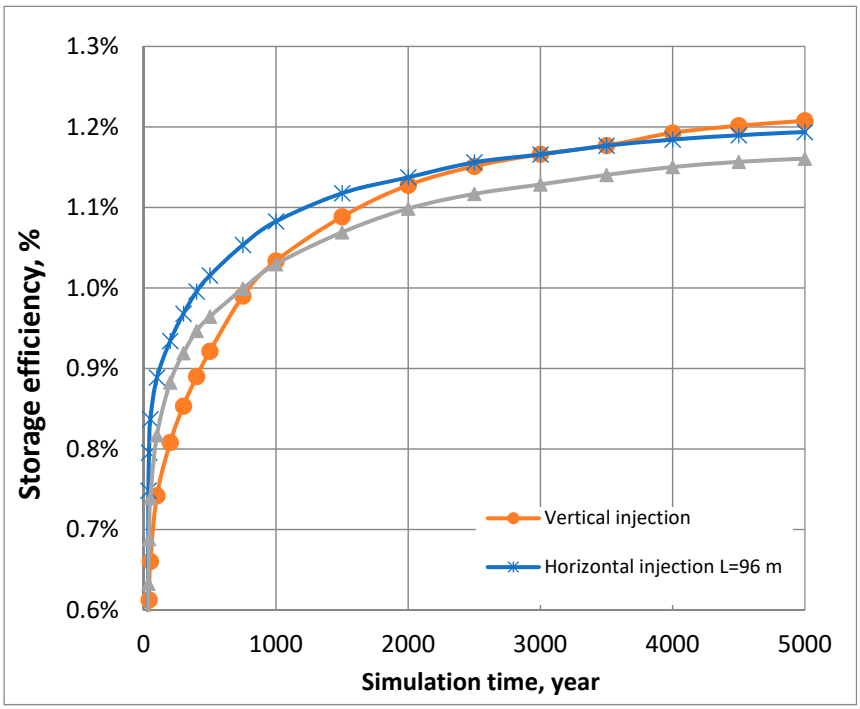

Figure 15. CO_2 storage efficiency for different injection orientation scenarios—cases 10, 11 and 12 in Table 3.

Additionally, the results reveal that horizontal injection into migration-controlled domains (i.e., open-boundary domains), returns slightly higher storage efficiency in short terms of simulation; however, after 2000 years, vertical injection methodology was found to be more efficient, as evidenced in Figure 15.

This is consistent with the findings by Okwen et al. [61], who suggest that using horizontal wells is preferable for pressure-limited domains and for sequestering large amounts of CO_2 in a short time frame. Accordingly, implementing longer horizontal injection wells does not significantly enhance the storage capacity and the economical factor has to be taken into consideration, should they need to be used for injecting large amounts of gas within limited periods of time.

3.7. Sensitivity to Domain Grid-Resolution

The grid discretization of any simulated domain is an important factor used to accurately capture the occurrence of different flow dynamics and assess the sensitivity of modelling results to the spatial gridding schemes. As mentioned earlier, in this study, two levels of grid refinement, a coarse grid ($88 \times 1 \times 24$) and a fine grid ($176 \times 1 \times 48$) were used to record the simulation code outputs (see cases 1 and 6 in Table 3).

The influence of the grid resolution is illustrated in Figure 16, where more detailed fingering maps of CO_2 dissolution can be observed in the fine-grid domain, compared to those for the coarse grid. Moreover, longer gas plumes were detected in the finer grid, which means that more accurate records of different forms of integrated gas were netted.

This is further evidenced in Figure 17A,B, in which it can be observed that, after 1500 years, a about 20% larger amount of dissolved gas and 54% lesser amount of free-gas were logged by the simulation code when a finer grid was implemented. These figures declined to about 1.3% and 3.2%, respectively, by the end of simulation. In Figure 17A, less impact of the grid resolution on CO_2 dissolution in the hosted brine was noted for both grids up to around 300 years of simulation. Then, after, an obvious increase in the dissolved gas trends for the finer grid, specifically between

800–2000 years, was noted. This deviancy diminishes after 2000 years, which agrees with the findings by Gonzalez-Nicolas et al. [62] and Bielinski [63].

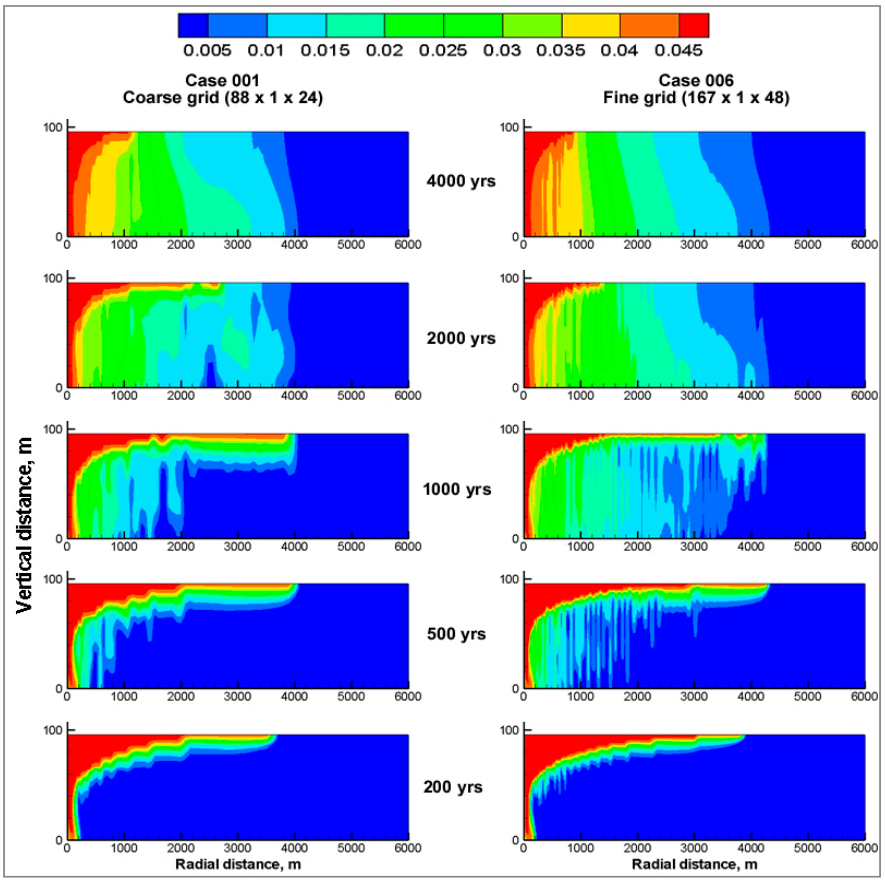

Figure 16. Aqueous CO_2 distribution in coarse and fine-grid homogeneous domains at different time scales.

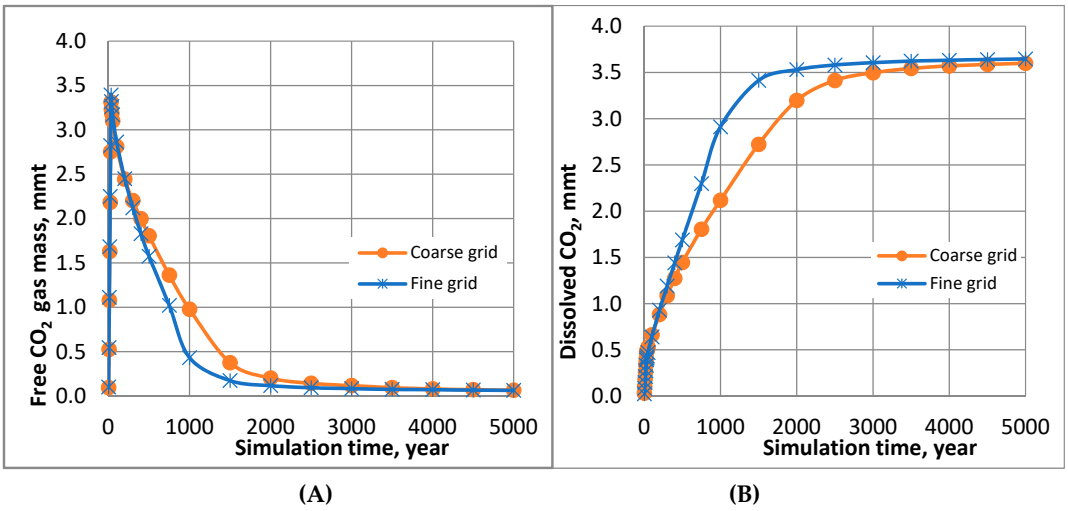

Figure 17. Effect of grid resolution for cases 5 and 6 in a homogeneous domain on: (**A**) dissolved CO_2; (**B**) free-gas CO_2.

This can be justified by the findings from this work (see Figure 15), which demonstrate the influence of grid resolution on the plume shape and number of formed fingers in the simulated domain

due to the convection forces and gravity instability. Consequently, more accurate results were logged using finer grids which justifies the relatively higher efficiency achieved in the case of fine-resolution grid, as illustrated in Figure 17.

Unexpectedly, the results revealed higher gas entrapment in the coarse grid (case 1) than that for the fine grid (case 6), as shown in Table 4. This can be due to the fact that, by using larger blocks in the computational domain, part of the dissolved CO_2 might have been logged either as a free or trapped gas, which can be explained from the relatively larger amounts of the latter two forms of the content gas in the case of coarse refinement. In spite of this significant overestimation of the netted values of the trapped gas in the coarse grid, the amount of the free gas was found to be less in the finer grid by about 3.2%, as displayed in Table 4. However, the increase in the storage efficiency factor was only about 0.1% using a finer grid, as shown in Figure 18, which further clarifies that the grid refinement has only a small impact on the simulation results. Additionally, the amount of the residually trapped gas was much smaller than the amount of the dissolved CO_2 shown in Table 4 and, moreover, this small amount of the trapped gas itself is subject to dissolution in medium over long time frames.

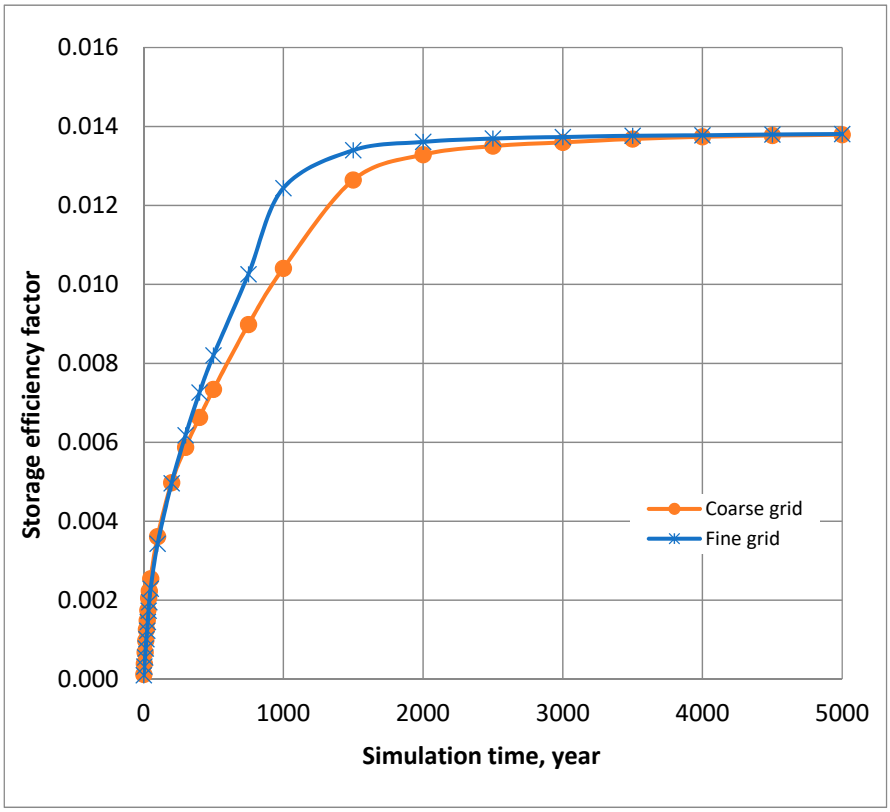

Figure 18. Grid refinement effect on CO_2 storage efficiency in a homogeneous domain. Cases 5 and 6 (Table 4).

Some preceding publications concluded only a slight or no impact of grid resolution on the simulation results. Conversely, ranking our simulation cases, according to the attribute of safer storage of the disposed gas in Table 4, the finer grid case was found to be on the top of the list. Therefore, and despite the excessive execution time required to conduct simulation runs with finer grids, it is important to magnify focus on the behaviour of the injected gas in different phases (i.e., dissolved, residually trapped and free-gas) within in situ pores network by using reasonably refined grids. The results from the finer mesh (see case 6 in Table 4) detected only about 0.497 MMT of free gas at the end of the simulation lifetime compared to about 0.514 MMT for the coarse grid in case 1, which reflects about 3.2% safer storage by the means of deploying the finer grid. This should be

motivating for the researchers to refine their modelling grids for further focused and more credible accurate results. Nevertheless, it is recommended that a sensible balance between the grid refinement and the computational time required for calculations be embraced.

For the cylindrical domain modelled in this research work (3 km radius and 96 m thickness), it was found that discretizing it to 176 by 48 nodes in the lateral and vertical direction, respectively, was found to provide a reasonably effective level of refinement in terms of balancing between the accuracy of the achieved results and the computational time and requirements.

4. Conclusions

A set of numerical simulation cases was developed and conducted using the STOMP-CO_2 numerical simulation code to investigate the influence of various types of heterogeneity, injection schemes, grid resolution, anisotropy, and injection orientation on the CO_2–water flow system behaviour and storage efficiency in saline aquifers. It was found that heterogeneous formations amplify the residual trapping mechanism, while CO_2 dissolution (i.e., solubility trapping mechanism) shows higher trends in homogeneous formations. However, overall, the heterogeneous media were found to be more effective in storing CO_2 safely over long-time frames. Compared to the homogeneous media, cyclic injection methodology has shown more influence on the heterogeneous domains through which the injected gas spreads out further, leading to greater interfacial area with brine and, consequently, escalating CO_2 dissolution. However, further research work is required to investigate more details about optimizing the injection times and pausing intervals in long-term sequestration projects where mineralization trapping plays an important role.

We observed that, while a CO_2 gas plume extends further at higher k_v/k_h values, lower ratios enhance the solubility trapping of CO_2 at early stages of simulation. Additionally, stronger hysteresis at higher permeability ratios enhances the residual trapping mechanism. Overall, storage efficiency increases proportionally with the permeability ratio of geological formations because higher ratios facilitate the further extent of the gas plume and increase the solubility trapping of the integrated gas. Using the maximum length of the gas plume in Equation (21) to calculate the available porous volume in open-boundary domains requires more investigation because it produced some unrealistic results. Therefore, an optimization is suggested to set up the domain length according to the employed injection rate or pressure, so that the extended gas plume just reaches but does not pass it. This length can be called the effective length and can be used to calculate the volume available to host the potential injected gas. It is also concluded in this study that employing longer horizontal wells does not increase storage efficiency. However, more research work is recommended to optimize the length of the horizontal wells and the injection techniques, including injecting chase brine along with scCO_2.

Despite the excessive execution time required to run simulations on finer-grid domains, it is important to magnify focus on the behaviour of the injected gas in order to increase the accuracy of the logged results. Finer-resolution grids can slightly increase the calculated values of the storage efficiency factor, specifically in the medium terms of sequestration. However, practical balance should be maintained between the refinement level and the computational requirements along with the execution time needed.

Author Contributions: Conceptualization, K.J.K. and D.B.D.; Methodology, K.J.K. and D.B.D.; Software, K.J.K.; Validation, K.J.K.; Formal Analysis, K.J.K. and D.B.D.; Investigation, K.J.K. and D.B.D.; Resources, K.J.K. and D.B.D.; Data Curation, K.J.K.; Writing-Original Draft Preparation, K.J.K.; Writing-Review & Editing, K.J.K. and D.B.D.; Visualization, K.J.K.; Supervision, D.B.D.; Project Administration, K.J.K. and D.B.D.; Funding Acquisition, K.J.K. and D.B.D. All authors have read and agreed to the published version of the manuscript.

Funding: This research received no external funding.

Acknowledgments: This work was part of a Doctoral Thesis Completed by the first author of this paper, supported by the Chemical Engineering Department, Loughborough University. Both authors would like to thank Mark D. White from Pacific Northwest National Laboratory (PNNL), USA, for his insight and helpful comments in employing the STOMP-CO_2 simulation code in this study.

Conflicts of Interest: The authors declare no conflict of interest.

References

1. IPCC. *Carbon Dioxide Capture and Storage*; IPCC Special Report; Cambridge University Press: Cambridge, UK, 2005; Volume 217.
2. Said, A.; Laukkanen, T.; Järvinen, M. Pilot-scale experimental work on carbon dioxide sequestration using steelmaking slag. *Appl. Energy* **2016**, *177*, 602–611. [CrossRef]
3. Ren, F.; Ma, G.; Wang, Y.; Fan, L.; Zhu, H. Two-phase flow pipe network method for simulation of CO_2 sequestration in fractured saline aquifers. *Int. J. Rock Mech. Min. Sci.* **2017**, *98*, 39–53. [CrossRef]
4. Cui, G.; Wang, Y.; Rui, Z.; Chen, B.; Ren, S.; Zhang, L. Assessing the combined influence of fluid-rock interactions on reservoir properties and injectivity during CO_2 storage in saline aquifers. *Energy* **2018**, *155*, 281–296. [CrossRef]
5. Jiang, L.; Xue, Z.; Park, H. Enhancement of CO_2 dissolution and sweep efficiency in saline aquifer by micro bubble CO_2 injection. *Int. J. Heat Mass Transf.* **2019**, *138*, 1211–1221. [CrossRef]
6. Singh, M.; Chaudhuri, A.; Chu, S.P.; Stauffer, P.H.; Pawar, R.J. Analysis of evolving capillary transition, gravitational fingering, and dissolution trapping of CO_2 in deep saline aquifers during continuous injection of supercritical CO_2. *Int. J. Greenh. Gas Control* **2019**, *82*, 281–297. [CrossRef]
7. Seo, S.; Mastiani, M.; Hafez, M.; Kunkel, G.; Asfour, C.G.; Garcia-Ocampo, K.I.; Kim, M. Injection of in-situ generated CO_2 microbubbles into deep saline aquifers for enhanced carbon sequestration. *Int. J. Greenh. Gas Control* **2019**, *83*, 256–264. [CrossRef]
8. Rasheed, Z.; Raza, A.; Gholami, R.; Rabiei, M.; Ismail, A.; Rasouli, V. A numerical study to assess the effect of heterogeneity on CO_2 storage potential of saline aquifers. *Energy Geosci.* **2020**, *1*, 1–2, 20–27. [CrossRef]
9. Khudaida, K.J.; Das, D.B. A numerical study of capillary pressure–saturation relationship for supercritical carbon dioxide (CO_2) injection in deep saline aquifer. *Chem. Eng. Res. Des.* **2014**, *92*, 3017–3030. [CrossRef]
10. Abidoye, L.K.; Khudaida, K.J.; Das, D.B. Geological carbon sequestration in the context of two-phase flow in porous media: A review. *Crit. Rev. Environ. Sci. Technol.* **2015**, *45*, 1105–1147. [CrossRef]
11. Kopp, A.; Class, H.; Helmig, R. Investigations on CO_2 storage capacity in saline aquifers—Part 2: Estimation of storage capacity coefficients. *Int. J. Greenh. Gas Control* **2009**, *3*, 277–287. [CrossRef]
12. Gough, C.; Shakley, S.; Holloway, S.; Bentham, M.; Bulatov, I.; McLachlan, C.; Klemes, J.; Purdy, R.; Cockerill, T. An integrated assessment of carbon dioxide capture and storage in the UK. In Proceedings of the 8th International Conference on Greenhouse Gas Control Technologies, Trondheim, Norway, 19–22 June 2006.
13. Bachu, S. Review of CO_2 storage efficiency in deep saline aquifers. *Int. J. Greenh. Gas Control* **2015**, *40*, 188–202. [CrossRef]
14. Jin, C.; Liu, L.; Li, Y.; Zeng, R. Capacity assessment of CO_2 storage in deep saline aquifers by mineral trapping and the implications for Songliao Basin, Northeast China. *Energy Sci. Eng.* **2017**, *5*, 81–89. [CrossRef]
15. Vilarrasa, V.; Bolster, D.; Olivella, S.; Carrera, J. Coupled hydromechanical modeling of CO_2 sequestration in deep saline aquifers. *Int. J. Greenh. Gas Control* **2010**, *4*, 910–919. [CrossRef]
16. Potdar, R.S.; Vishal, V. Trapping Mechanism of CO_2 Storage in Deep Saline Aquifers: Brief Review. In *Geologic Carbon Sequestration*; Springer: Cham, Switzerland, 2016; pp. 47–58.
17. Khan, S.; Khulief, Y.A.; Al-Shuhail, A. Mitigating climate change via CO_2 sequestration into Biyadh reservoir: Geomechanical modeling and caprock integrity. *Mitig. Adapt. Strateg. Glob. Chang.* **2019**, *24*, 23–52. [CrossRef]
18. Goodarzi, S.; Settari, A.; Ghaderi, S.M.; Hawkes, C.; Leonenko, Y. The effect of site characterization data on injection capacity and cap rock integrity modeling during carbon dioxide storage in the Nisku saline aquifer at the Wabamun Lake area, Canada. *Environ. Geosci.* **2020**, *27*, 49–65. [CrossRef]
19. Gorecki, C.D.; Sorensen, J.A.; Bremer, J.M.; Ayash, S.C.; Knudsen, D.J.; Holubnyak, Y.I.; Harju, J.A. Development of Storage Coefficients for determining Carbon Dioxide Storage in Deep Saline Formations. In Proceedings of the SPE International Conference on CO_2 Capture, Storage, and Utilization, San Diego, CA, USA, 2–4 November 2009.
20. Knopf, S.; May, F. Comparing methods for the estimation of CO_2 storage capacity in saline aquifers in Germany: Regional aquifer based vs. structural trap based assessments. *Energy Procedia* **2017**, *114*, 4710–4721. [CrossRef]
21. Pingping, S.; Xinwei, L.; Qiujie, L. Methodology for estimation of CO_2 storage capacity in reservoirs. *Pet. Explor. Dev.* **2009**, *36*, 216–220. [CrossRef]

22. Kim, Y.; Jang, H.; Kim, J.; Lee, J. Prediction of storage efficiency on CO_2 sequestration in deep saline aquifers using artificial neural network. *Appl. Energy* **2017**, *185*, 916–928. [CrossRef]
23. Zhou, Q.; Birkholzer, J.T.; Tsang, C.; Rutqvist, J. A method for quick assessment of CO_2 storage capacity in closed and semi-closed saline formations. *Int. J. Greenh. Gas Control* **2008**, *2*, 626–639. [CrossRef]
24. Frailey, S.M. Methods for estimating CO_2 storage in saline reservoirs. *Energy Procedia* **2009**, *1*, 2769–2776. [CrossRef]
25. Ehlig-Economides, C.; Economides, M.J. Sequestering carbon dioxide in a closed underground volume. *J. Pet. Sci. Eng.* **2010**, *70*, 123–130. [CrossRef]
26. Macminn, C.W.; Juanes, R. A mathematical model of the footprint of the CO_2 plume during and after injection in deep saline aquifer systems. *Energy Procedia* **2009**, *1*, 3429–3436. [CrossRef]
27. Kopp, A.; Class, H.; Helmig, R. Investigations on CO_2 storage capacity in saline aquifers: Part 1. Dimensional analysis of flow processes and reservoir characteristics. *Int. J. Greenh. Gas Control* **2009**, *3*, 263–276. [CrossRef]
28. Okwen, R.T.; Stewart, M.T.; Cunningham, J.A. Analytical solution for estimating storage efficiency of geologic sequestration of CO_2. *Int. J. Greenh. Gas Control* **2010**, *4*, 102–107. [CrossRef]
29. Kopp, A.; Probst, P.; Class, H.; Hurter, S.; HELMIG, R. Estimation of CO_2 storage capacity coefficients in geologic formations. *Energy Procedia* **2009**, *1*, 2863–2870. [CrossRef]
30. Yang, F.; Bai, B.; Tang, D.; Shari, D.; David, W. Characteristics of CO_2 sequestration in saline aquifers. *Pet. Sci.* **2010**, *7*, 83–92. [CrossRef]
31. Goodman, A.; Bromhal, G.; Strazisar, B.; Rodosta, T.; Guthrie, W.F.; Allen, D.; Guthrie, G. Comparison of methods for geologic storage of carbon dioxide in saline formations. *Int. J. Greenh. Gas Control* **2013**, *18*, 329–342. [CrossRef]
32. Anderson, S.T.; Jahediesfanjani, H. Estimating the pressure-limited dynamic capacity and costs of basin-scale CO_2 storage in a saline formation. *Int. J. Greenh. Gas Control* **2019**, *88*, 156–167. [CrossRef]
33. Goodman, A.; Hakala, A.; Bromhal, G.; Deel, D.; Rodosta, T.; Frailey, S.; Guthrie, G. US DOE methodology for the development of geologic storage potential for carbon dioxide at the national and regional scale. *Int. J. Greenh. Gas Control* **2011**, *5*, 952–965. [CrossRef]
34. Szulczewski, M.L. The Subsurface Fluid Mechanics of Geologic Carbon Dioxide Storage. Ph.D. Thesis, Massachusetts Institute of Technology, Cambridge, MA, USA, 2013; pp. 32–38.
35. Chasset, C.; Jarsjö, J.; Erlström, M.; Cvetkovic, V.; Destouni, G. Scenario simulations of CO_2 injection feasibility, plume migration and storage in a saline aquifer, Scania, Sweden. *Int. J. Greenh. Gas Control* **2011**, *5*, 1303–1318. [CrossRef]
36. Birkholzer, J.T.; Zhou, Q.; Tsang, C. Large-scale impact of CO_2 storage in deep saline aquifers: A sensitivity study on pressure response in stratified systems. *Int. J. Greenh. Gas Control* **2009**, *3*, 181–194. [CrossRef]
37. Jikich, S.A.; Sams, W.N.; Bromhal, G.; Pope, G.; Gupta, N.; Smith, D.H. Carbon dioxide injectivity in brine reservoirs using horizontal wells. In Proceedings of the 2nd Annual Conference on Carbon Sequestration, Pittsburgh, PA, USA, 5–8 May 2003.
38. Ghaderi, S.; Keith, D.; Leonenko, Y. Feasibility of injecting large volumes of CO_2 into aquifers. *Energy Procedia* **2009**, *1*, 3113–3120. [CrossRef]
39. De Silva, P.N.K.; Ranjith, P.G. A study of methodologies for CO_2 storage capacity estimation of saline aquifers. *Fuel* **2012**, *93*, 13–27. [CrossRef]
40. Vilarrasa, V. Impact of CO_2 injection through horizontal and vertical wells on the caprock mechanical stability. *Int. J. Rock Mech. Min. Sci.* **2014**, *66*, 151–159. [CrossRef]
41. Hassanzadeh, H.; Pooladi-Darvish, M.; Keith, D. Accelerating CO_2 Dissolution in Saline Aquifers for Geological Storage—Mechanistic and Sensitivity Studies. *Energy Fuels* **2009**, *23*, 3328–3336. [CrossRef]
42. White, M.D.; Watson, D.J.; Bacon, D.H.; White, S.K.; Mcgrail, B.P.; Zhang, Z.F. *Stomp- Subsurface Transport Over Multiple Phases- STOMP- CO_2 and—CO_2e Guide*; V 1.1: 1.1–5.66; Pacific Northwest National Laboratory: Richland, WA, USA, 2013.
43. Holtz, M.H. Residual gas saturation to aquifer influx: A calculation method for 3-D computer reservoir model construction. In Proceedings of the SPE Gas Technology Symposium, Calgary, AB, Canada, 30 April–2 May 2002.
44. Khudaida, K.J. Modelling CO_2 Sequestration in Deep Saline Aquifers. Ph.D. Thesis, Loughborough University, Loughborough, UK, 2016; pp. 46–47.

45. Span, R.; Wagner, W. A new equation of state for carbon dioxide covering the fluid region from the triple-point temperature to 1100 K at pressures up to 800 MPa. *J. Phys. Chem. Ref. Data* **1996**, *25*, 1509–1596. [CrossRef]
46. Giljarhus, K.E.T.; Munkejord, S.T.; Skaugen, G. Solution of the Span–Wagner equation of state using a density–energy state function for fluid-dynamic simulation of carbon dioxide. *Ind. Eng. Chem. Res.* **2011**, *51*, 1006–1014. [CrossRef]
47. Spycher, N.; Pruess, K.; Ennis-King, J. CO_2 -H_2O mixtures in the geological sequestration of CO_2. I. Assessment and calculation of mutual solubilities from 12 to 100 °C and up to 600 bar. *Geochim. Cosmochim. Acta* **2003**, *67*, 3015–3031. [CrossRef]
48. Spycher, N.; Pruess, K. A phase-partitioning model for CO_2–brine mixtures at elevated temperatures and pressures: Application to CO_2-enhanced geothermal systems. *Transp. Porous Media* **2010**, *82*, 173–196. [CrossRef]
49. Van Genuchten, M.T. A closed-form equation for predicting the hydraulic conductivity of unsaturated soils. *Soil Sci. Soc. Am. J.* **1980**, *44*, 892–898. [CrossRef]
50. Kaluarachchi, J.J.; Parker, J.C. Multiphase flow with a simplified model for oil entrapment. *Transp. Porous Media* **1992**, *7*, 1–14. [CrossRef]
51. Land, C.S. Calculation of imbibition relative permeability for two- and three-phase flow from rock properties. *Trans. Am. Inst. Min. Metall. Pet. Eng* **1968**, *243*, 149–156. [CrossRef]
52. Mualem, Y. A new model for predicting the hydraulic conductivity of unsaturated porous media. *Water Resour. Res.* **1976**, *12*, 513–522. [CrossRef]
53. White, M.D.; Oostrom, M.; Lenhard, R.J. A Practical Model for Mobile, Residual, and Entrapped NAPL in Water-Wet Porous Media. *Groundwater* **2004**, *42*, 734–746. [CrossRef] [PubMed]
54. Birkholzer, J.T.; Zhou, Q.; Rutqvist, J.; Jordan, P.; Zhang, K.; Tsang, C. *Research Project on CO2 Geological Storage and Groundwater Resources: Large-Scale Hydrogeological Evaluation and Impact on Groundwater Systems*; Report LBNL-63544; Lawrence Berkeley National Laboratory: Berkeley, CA, USA, 2007; pp. 20–31.
55. Szulczewski, M.L.; Macminn, C.W.; Juanes, R. How pressure buildup and CO_2 migration can both constrain storage capacity in deep saline aquifers. *Energy Procedia* **2011**, *4*, 4889–4896. [CrossRef]
56. Szulczewski, M.L. Storage Capacity and Injection Rate Estimates for CO_2 Sequestration in Deep Saline Aquifers in the Conterminous United States. Ph.D. Thesis, Massachusetts Institute of Technology, Cambridge, MA, USA, 2009; pp. 38–51.
57. Alabi, O.O. Fluid flow in homogeneous and heterogeneous porous media. *Electron. J. Geotech. Eng.* **2011**, *16*, 61–70.
58. Zhao, X.; Liao, X.; Wang, W.; Chen, C.; Rui, Z.; Wang, H. The CO_2 storage capacity evaluation: Methodology and determination of key factors. *J. Energy Inst.* **2014**, *87*, 297–305. [CrossRef]
59. Juanes, R.; Spiteri, E.J.; Orr, F.M.; Blunt, M.J. Impact of relative permeability hysteresis on geological CO_2 storage. *Water Resour. Res.* **2006**, *42*. [CrossRef]
60. Widarsono, B.; Muladi, A.; Jaya, I. Vertical–Horizontal Permeability Ratio in Indonesian Sanstone and Carbonate Reservoirs. In Proceedings of the Simposium Nasional IATMI, Yogyakarta, Indonesia, 25–28 July 2007.
61. Okwen, R.; Stewart, M.; Cunningham, J. Effect of well orientation (vertical vs. horizontal) and well length on the injection of CO_2 in deep saline aquifers. *Transp. Porous Media* **2011**, *90*, 219–232. [CrossRef]
62. Gonzalez-Nicolas, A.; Cody, B.; Baù, D. Numerical simulation of CO_2 injection into deep saline aquifers. In Proceedings of the AGU Hydrology Days, Fort Collins, CO, USA, 21–23 March 2011; pp. 107–113.
63. Bielinski, A. Numerical Simulation of CO_2 Sequestration in Geological Formations. Ph.D. Thesis, University of Stuttgart, Stuttgart, Germany, 2007.

© 2020 by the authors. Licensee MDPI, Basel, Switzerland. This article is an open access article distributed under the terms and conditions of the Creative Commons Attribution (CC BY) license (http://creativecommons.org/licenses/by/4.0/).